Biaxial behavior and design of steel-concrete composite columns

A Thesis Presented for the
Master of Science
Degree
The University of Tennessee, Knoxville

Amirfarzad Behnam
December 2020

DEDICATION

I dedicate this thesis to my wife Shabnam

ACKNOWLEDGEMENTS

I would like to thank my supervisor Dr. Mark Denavit for his consistent support and guidance during the running of this project. Also, I would like to express my appreciation to my committee members Dr. Timothy Truster and Dr. Nicholas Wierschem. Furthermore, I would like to thank all the staff and services of the Department of Civil and Environmental Engineering department at the University of Tennessee, Knoxville.

ABSTRACT

Steel-concrete composite columns are efficient structural members that possess significant strength, stiffness, and ductility. Accurate methods of assessing the strength of these members are necessary to realize their benefits. Several design codes rely on the plastic stress distribution method (PSD) for computing the cross-sectional strength of composite columns subjected to axial compression and flexural bending. However, there has been limited validation of this method over the wide range of material and geometric properties and loading conditions to which it is permitted to be applied. The first part of this thesis presents a study of the behavior of short composite columns and methods of evaluating their strength. The usage of the PSD method and the strain compatibility method is validated against detailed fiber cross section analyses and published experimental data. The results indicate that the PSD method can yield significantly unconservative strength predictions, especially for encased composite members with high steel yield strengths and high steel ratios. A simple modification factor which can be applied to the results of the PSD method to achieve greater accuracy was derived. This modification factor is suitable for use in design practice and enables better predictions of the strength of short composite columns. The second part focuses on the biaxial strength and design of these members including length effects. Current provisions regarding the strength of composite columns under combined axial compression and biaxial bending are overly simplistic and conservative. This thesis presents a study of the biaxial behavior of composite columns and methods of evaluating their strength. Analyses of composite cross sections confirm the conservative nature of current design provisions and form the basis for modified strength equations that better capture the shape of three-dimensional interaction surface, and confirm that the proposed design equations are suitable for use within the direct analysis method for evaluating members with length effects. The proposed design equations are further validated against published experimental results. This work advances understanding of the behavior of composite columns

subjected to axial compression and biaxial bending and present improved yet practical methods of evaluating strength under these conditions that will enable more efficient designs.

TABLE OF CONTENTS

LIST OF TABLES

LIST OF FIGURES

List of Symbols

A_c	Area of concrete
A_g	Gross area of cross section
A_s	Area of steel shape
A_{sr}	Area of reinforcement
B	Outside width of the cross section
D	Outside diameter of the cross section
d_b	Reinforcing bar diameter
E	Modulus of elasticity of steel
f'_c	Concrete compressive strength
F_y	Steel yield strength
F_{ysr}	Reinforcement yield strength
H	Outside height of the cross section
L	Column length
M_{ISA}	Flexural moment strength from inelastic section analysis
M_{no}	Resultant nominal flexural moment from the PSD method
$M_{no,x}$	Nominal flexural moment strength about x-axis from the PSD method
$M_{no,y}$	Nominal flexural moment strength about y-axis from the PSD method
M_{PSD}	Flexural moment strength from plastic stress distribution
M_{SC}	Flexural moment strength from strain compatibility method
M_x	Flexural moment strength about x-axis
M_y	Flexural moment strength about y-axis
M_θ	Resultant flexural moment strength in loading angle θ
P	Axial load
P_{no}	Nominal cross-sectional axial strength
r_1	Radial distance of curve 1 from origin
r_2	Radial distance of curve 2 from origin
r_{ISA}	Radial distance of ISA interaction curve from origin
r_{PSD}	Radial distance of PSD interaction curve from origin
r_{SC}	Radial distance of SC interaction curve from origin
t	Thickness of the steel tube
ε	Error calculated between two interaction strength curves
θ	Loading angle
ρ_s	Steel ratio (= A_s/A_g)
φ_1	Regression parameter for modification factor
φ_2	Regression parameter for modification factor
ψ	Modification factor

INTRODUCTION

Steel-concrete composite columns exhibit excellent behavior and strength by efficiently combining the advantages of structural steel and reinforced concrete. Steel reinforced concrete (SRC) and concrete-filled steel tube (CFT) are the two main classifications of steel-concrete composite columns. There have been several recent advances in the evaluation of strength of composite columns including consideration of CFT with thin tubes subject to local buckling (Lai et al. 2014; Lai and Varma 2015) and explicit frame stability provisions (Denavit et al. 2016a), however several studies have reported some inaccuracies in the main methodologies presented in the design codes like the *AISC Specification* (2016) which are not resolved yet as there are very limited studies investigating the behavior of these members and the accuracy of the established methodologies over a wide range of material and cross-sectional properties. For instance, Denavit and Hajjar (2014) reported significant unconservative errors in minor-axis bending of SRC members evaluated via the plastic stress distribution method. Also, several studies have shown that steel-concrete composite members maintain most of their uniaxial flexural strength when they are subjected to biaxial bending (Morino et al. 1984a; Virdi et al. 1973); however, an overly conservative method of determining the available strength in these conditions is presented in the commentary of the *AISC Specification* (2016). So, a comprehensive investigation of the available design methodologies in the design codes, and a study of three-dimensional behavior of composite columns under biaxial flexure and axial compression are two aspects that warrant further study.

The first chapter of this thesis targets the first aspect. The plastic stress distribution (PSD) and strain compatibility (SC) methods that are presented in the *AISC Specification* (2016) as the main methodologies for determining the strength of these members, are evaluated over a wide range of material and cross-sectional properties via comparisons to the accurately modeled inelastic section analyses. These comparisons demonstrated that the plastic stress distribution method exhibits some unconservative errors, especially for SRC members. A simple modification is proposed and calibrated against the results of the parametric study to mitigate the unconservative error that occurs when evaluating the strength of these members by the plastic stress distribution method. A comparison between the current and proposed methods of strength evaluation against the previously published experimental results is also presented. This validation confirmed that the plastic stress distribution method overestimates the strength for some cross sections and that the proposed modification to this method improves the accuracy to an acceptable level.

While the proposed modification developed in the first chapter improves the plastic stress distribution method in terms of unconservative errors, the simplistic approach for evaluation of the biaxial bending strength of these members in the commentary of the *AISC Specification* (2016), which is based on some anchor points from the plastic stress distribution method requires further attention. In the second chapter, the focus is on the biaxial behavior and strength of steel-concrete composite members. In the first part of the chapter, the interaction strength equations for determining the strength of composite cross sections are revisited and a parametric study is performed to interpret the shape of the three-dimensional interaction surface and the factors influence it. An improved, yet simple, strength interaction equation is proposed with a governing shape parameter calibrated against the results of the parametric study. In the second part of this chapter, the stability behavior of steel-concrete composite beam-columns are investigated, and design recommendations proposed for such beam-columns in biaxial flexure are evaluated. For this purpose, an extensive three-dimensional benchmark study is carried out in order to perform comparisons between second-order inelastic results and results from the proposed design methodology. The benchmark frames are expanded to target several out of plane stability issues such as different frame types in major and minor axis, and initial imperfections in a direction with the most destabilizing effect. Then, the proposed interaction equation is also validated against published experimental results. These comparisons demonstrated that the proposed interaction equation is suitable for use within the direct analysis method as defined in the AISC *Specification* (2016), especially when used in conjunction with anchor points computed using a modified version of the plastic stress distribution method.

References

AISC. (2016). *Specification for structural steel buildings*. American Institute of Steel Construction, Chicago, Illinois.

Denavit, M. D., and Hajjar, J. F. (2014). *Characterization of Behavior of Steel-Concrete Composite Members and Frames with Applications for Design*. Newmark Structural Laboratory Report Series, Newmark Structural Laboratory Report NSEL-034, University of Illinois at Urbana-Champaign, Urbana, Illinois.

Denavit, M. D., Hajjar, J. F., Perea, T., and Leon, R. T. (2016). "Stability Analysis and Design of Composite Structures." *Journal of Structural Engineering*, ASCE, 142(3), 04015157.

Lai, Z., and Varma, A. H. (2015). "Noncompact and slender circular CFT members: Experimental database, analysis, and design." *Journal of Constructional Steel Research*, 106, 220–233.

Lai, Z., Varma, A. H., and Zhang, K. (2014). "Noncompact and slender rectangular CFT members: Experimental database, analysis, and design." *Journal of Constructional Steel Research*, 101, 455–468.

Morino, S., Matsui, C., and Watanabe, H. (1984). "Strength of biaxially loaded SRC columns." 185–194.

Virdi, K. S., Pilkington, J., Dowling, P., and Croft, D. (1973). "Discussion. The ultimate strength of composite columns in biaxial bending." *Proceedings of the institution of civil engineers*, 55, 739–741.

CHAPTER 1

PLASTIC STRESS DISTRIBUTION METHOD FOR PREDICTING INTERACTION STRENGTH OF STEEL-CONCRETE COMPOSITE CROSS SECTIONS

A version of this chapter was originally published by Amirfarzad Behnam and Mark D. Denavit:

Behnam, Amirfarzad, and Mark D. Denavit. "Plastic stress distribution method for predicting interaction strength of steel-concrete composite cross sections." *Journal of Constructional Steel Research* 170 (2020): 106092.

The research performed in this paper was done by Amirfarzad Behnam under supervision of Dr. Mark Denavit at the Department of Civil and Environmental Engineering, University of Tennessee, Knoxville. The first manuscript of the paper was peer-reviewed by three researchers and lightly revised to address their comments and recommendations.

Abstract

Steel-concrete composite columns are efficient structural members that possess significant strength, stiffness, and ductility. Accurate methods of assessing the strength of these members are necessary to realize their benefits. Several design codes rely on the plastic stress distribution method for computing the cross-sectional strength of composite columns subjected to axial compression and flexural bending. However, there has been limited validation of this method over the wide range of material properties, cross-sectional geometries, and loading conditions to which it is permitted to be applied. This chapter presents a study of the behavior of short composite columns and methods of evaluating their strength. The use of the plastic stress distribution method and the strain compatibility method to evaluate the strength of composite columns is validated against detailed fiber cross section analyses and published experimental data. The results of this study indicate that the plastic stress distribution method can yield significantly unconservative strength predictions, especially for encased composite members with high steel yield strengths and high steel ratios. Motivated by these results, a simple modification factor which can be applied to the results of the plastic stress distribution method to achieve greater accuracy was derived. This modification factor is suitable for use in

design practice and enables better predictions of the strength of short composite columns.

Keywords: Composite Beam-columns; Strength Interaction; Steel-Concrete Composite; Design

Introduction

Steel-concrete composite columns have been shown to exhibit excellent structural behavior and are an effective alternative to more traditional structural steel or reinforced concrete columns. There are two general categories of steel-concrete composite column: concrete encased members, also known as steel reinforced concrete (SRC) members; and concrete-filled members, also known as concrete-filled steel tube (CFT) members. Concrete-filled steel tube members are further categorized by the shape of the steel tube, which is usually either circular (CCFT) or rectangular (RCFT). Typical cross sections for these composite members are shown in Figure 1-1.

There have been significant advances in both the fundamental understanding of the strength of steel-concrete composite beam-columns and corresponding design provisions recently. When first introduced to the AISC Specification, the strength of composite beam-columns was computed based on an equivalent steel cross section (AISC 1986). This was changed in the 2005 edition of the Specification (AISC 2005), when the provisions were revised to calculate the strength in a more mechanistic manner. Specifically, the plastic stress distribution (PSD) and strain compatibility (SC) methods were introduced for computing the strength of composite column cross sections. Other standards, including the Eurocode (CEN 2004) and the Chinese code for composite structures (SAC 2014), also use the PSD method for determining the strength of steel-concrete composite members. The PSD method has been validated against available experimental data (Leon et al. 2007), however, it has not been systematically evaluated over the range of materials, cross-sectional geometries, and loading conditions permitted by the AISC Specification.

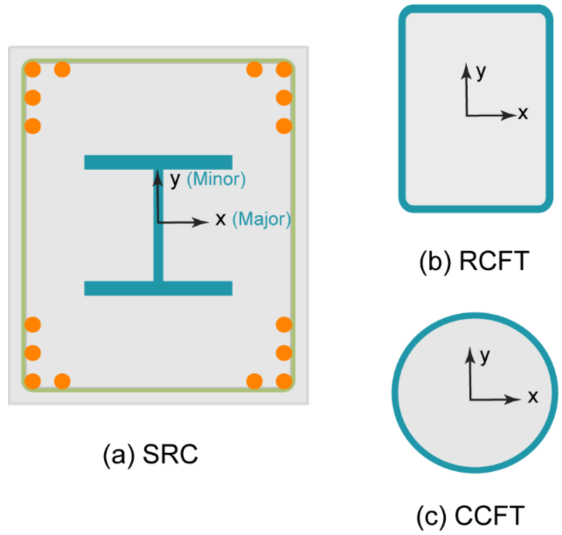

Figure 1-1. Typical steel-concrete composite cross sections

The behavior and design of steel-concrete composite members has been investigated in many previous studies. Thousands of experiments on composite columns have been performed (Kim 2005; Goode 2008a; Gourley et al. 2008b). Experimental studies on CFT members subjected to axial compression and flexure, such as Fujimoto et al. (2008) and Varma et al. (2002), have shown that short members exhibit yielding of the steel tube and crushing of the concrete at failure. Local buckling of the steel tube has also been observed, either after the peak load is attained for thicker tubes or earlier for thinner tubes. Experimental studies on SRC members, such as Virdi and Dowling (1973) and Ricles and Paboojian (1994), have shown that short members exhibit yielding of the steel shape and crushing of the concrete at failure. The concrete has been shown to effectively prevent local buckling of the steel shape, however, spalling of the cover concrete may occur after the peak is attained. These observations have been incorporated into a variety of numerical models and stress-strain relationships for the behavior of composite columns (Sakino et al. 2004; Hatzigeorgiou 2008; Denavit and Hajjar 2014; Lai and Varma 2016).

This work presents a study of the behavior of steel-concrete composite cross sections with a focus on strength. Various approaches for determining the strength of composite cross sections are reviewed and evaluated against each other through a broad parametric study. Noting unconservative error stemming from the PSD method, a simple modification to increase accuracy is proposed and calibrated against the results of the parametric study. Finally, the current methods and proposed modification are validated against previously published experimental results.

Current Design Provisions

The AISC Specification (AISC 2016) is the primary standard governing structural design of steel-concrete composite columns for building structures in the United States. It describes several methods for determining the strength of composite cross sections. The two main approaches are the PSD method and the SC method. Both of these methods are described below and illustrated for an example RCFT cross section consisting of a rectangular tube with outside height, H = 300 mm, outside width, B = 200 mm, thickness, t = 6.3 mm (this corresponds to a ratio of steel area to a gross area of $\rho_s = A_s/A_g = 0.1$), steel yield strength, F_y = 345 MPa, and concrete strength, f'_c = 20 MPa. The cross section has no internal reinforcing.

Plastic Stress Distribution (PSD) Method

To compute strength according to the PSD method, the entire steel cross section and all reinforcing bars (if present) are assumed to have attained their yield stress in either tension or compression and the concrete in compression is assumed to have attained stress of $0.85f'_c$ or $0.95f'_c$ for CCFT. The tension strength of concrete is neglected. The moments and axial load are obtained by integrating the assumed stresses over the cross-sectional area. An interaction diagram is obtained by computing the moments and axial load for many different positions and orientations of the neutral axis.

Steel is a highly ductile material that holds its capacity well beyond yield. In contrast, the strength of concrete typically declines after attaining its peak capacity. Therefore, the PSD method essentially assumes that the steel component achieves its peak capacity at the same time or before the concrete component does.

Closed-form equations are provided in the AISC Manual (AISC 2017) to compute key points within the interaction diagram. A fiber discretization approach to the PSD method is used in this work to accommodate a wider range of cross sections and loading conditions. The three-dimensional (P-M_x-M_y space) interaction strength diagram for the example RCFT cross section described above is shown in Figure 1-2a. Two-dimensional (M_x-M_y space) slices of the interaction diagram at three different axial loads are shown in Figure 1-3.

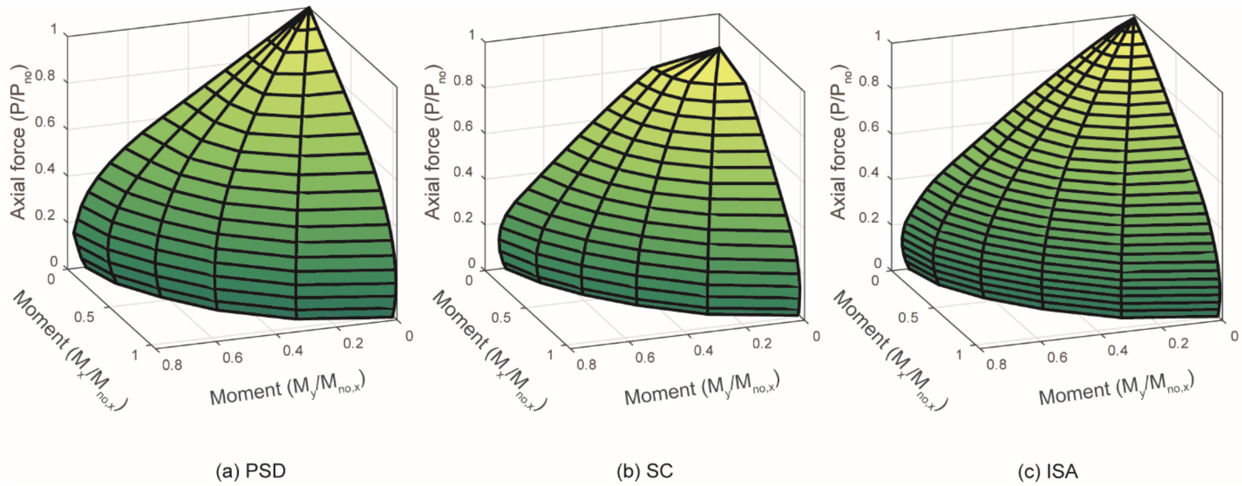

Figure 1-2. Three-dimensional interaction diagrams for example RCFT cross section

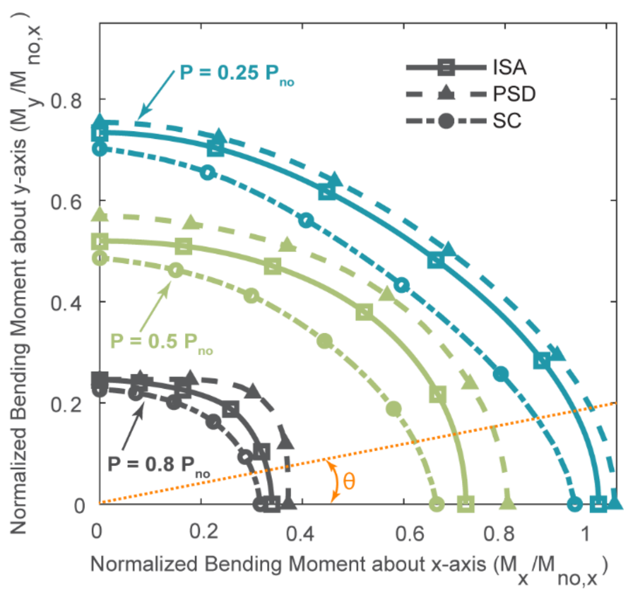

Figure 1-3. Two-dimensional interaction diagrams for example RCFT cross section

Strain Compatibility (SC) Method

The SC method is the main procedure for computing interaction diagrams following the ACI Code (ACI 2019). It is permitted as an alternative procedure within the AISC Specification (AISC 2016). The use of the SC method is specifically recommended for irregular cross sections and when the steel does not exhibit elasto-plastic behavior. In this method, the strain in the extreme concrete compressive fiber is assumed to be 0.003 with a linear distribution through the cross section. The steel and concrete stresses are computed from assumed stress-strain relationships and the moments and axial load are computed through integration over the cross section. The assumed stress-strain relationships should have a basis in experimental testing. For this work, an elastic-perfectly plastic relationship is used for the steel and the rectangular stress block described in the ACI Code is used for the concrete. Alternative stress blocks have been proposed as more appropriate for high-strength concrete (ACI 2018), however, for simplicity, these are not used in this work. An upper limit on compressive strength is required for reinforced concrete members in the ACI Code. A similar limit is commonly applied to steel-concrete composite members (Griffis 1992). In this work, the axial compressive strength for interaction diagrams computed using the SC method is capped at $0.8P_{no}$, where P_{no} is the axial capacity of the composite cross section defined by Equation 1-1. Note that Equation 1-1b and 1-1c apply only to filled composite members that are not subject to local buckling and do not have internal reinforcing.

$$P_{no} = F_y A_s + F_{ysr} A_{sr} + 0.85 f_c' A_c \quad \text{(SRC)} \tag{1-1a}$$

$$P_{no} = F_y A_s + 0.85 f_c' A_c \quad \text{(RCFT)} \tag{1-1b}$$

$$P_{no} = F_y A_s + 0.95 f_c' A_c \quad \left(\text{CCFT}\right) \tag{1-1c}$$

where, A_s, A_{sr}, and A_c are the cross-sectional areas of the steel shape, reinforcing bars, and concrete, respectively, and F_{ysr} is the yield stress of the reinforcing bars.

The three-dimensional interaction strength diagram for the example RCFT cross section described above is shown in Figure 1-2b. Two-dimensional slices of the interaction diagram at three different axial loads are shown in Figure 1-3. Given the selected stress-strain relationships, the strength according to the SC method is always less than that of the PSD method.

Inelastic Section Analysis

Inelastic section analysis (ISA) is another means of evaluating the strength of composite cross sections that has been shown to be accurate in comparison to experimental results (Sanz Picon 1992; Denavit and Hajjar 2014; Liang 2008; Patel et al. 2015). For the inelastic analyses performed in this work, the composite cross section is discretized into a grid of fibers with each assigned a uniaxial stress-strain relationship. The analyses are performed using the OpenSees framework (McKenna et al. 2010a) with a zero-length element and uniaxial constitutive relations defined specifically for steel-concrete composite cross sections.

For SRC cross sections, the section is discretized into 5 regions: 1) the wide-flange steel shape, 2) the highly confined concrete between the flanges of the steel shape, 3) the moderately confined concrete within the ties, 4) the cover concrete, and 5) the reinforcing steel bars (Figure 1-4a). Elastic-perfectly plastic materials are assigned to the steel components. Initial stresses are assigned to the steel shape to represent residual stresses following the Lehigh pattern (Galambos and Ketter 1959). The Popovics concrete stress-strain relationship is assigned to the three concrete regions with varying levels of confinement calculated based on the properties and geometry of the steel components (Denavit and Hajjar 2014).

For RCFT cross sections, the section is discretized into 3 regions: 1) the corners of the steel tube, 2) the flats of the steel tube, and 3) the concrete core (Figure 1-4b). The steel model used for RCFT cross sections is based on

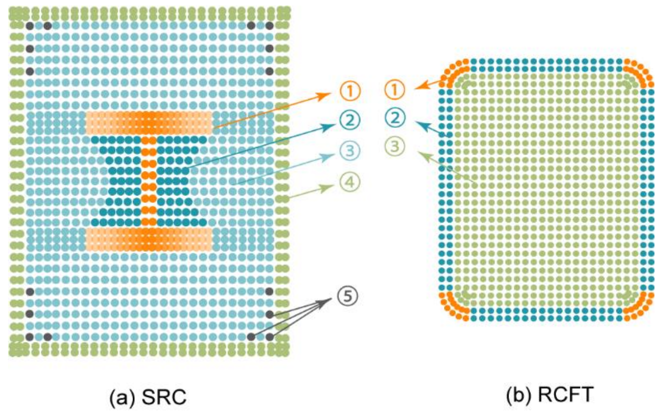

Figure 1-4. Example fiber section discretization

the work of Abdel-Rahman and Sivakumaran (1997) which captures residual stress and gradual variation to the plastic state through a multi-linear stress-strain relationship. The Popovics concrete stress-strain relationship is assigned to the concrete region without any enhancement from confinement (i.e., f'_c is the peak compressive stress).

For the CCFT cross sections, the section is discretized into 2 regions: 1) the steel tube and 2) the concrete core. The Abdel-Rahman and Sivakumaran (1997) model was used for the steel tube. The Popovics concrete stress-strain relationship is assigned to the concrete region with confinement based on the properties and geometry of the steel tube (Denavit and Hajjar 2014).

The maximum size of each fiber is taken as 1/30th of the outside dimension of the gross section along each of the principal axes. Each component of the cross section was discretized consistently with its assumed geometry such that the cross-sectional area of the fiber section was identical to that of the assumed geometry and the moment of inertia of the fiber section approached that of the assumed geometry as the size of the fibers decreased. Examples of the fiber discretization are shown in Figure 1-4. Studies (e.g., Kostic and Filippou 2012) have shown that a far more coarse discretization can achieve sufficiently accurate results. The fine discretization used in this work was selected based on a refinement study to achieve high accuracy.

The accuracy of these fiber sections and constitutive relations has been validated against the results of hundreds of experimental tests on composite members with various material and geometric properties and subjected to various loading conditions (Denavit and Hajjar 2014). A sample of the validation studies is presented in Figure 1-5, which shows experimental and numerical results for the IV series of specimens tested by Tomii and Sakino (1979). This series of specimens consisted of 7 nominally identical short RCFT beam-columns. The specimens were subjected to constant axial compression, the value of which varied between specimens from zero to 376 kN, and increasing bending moment until failure. The steel tubes were square with outside width of

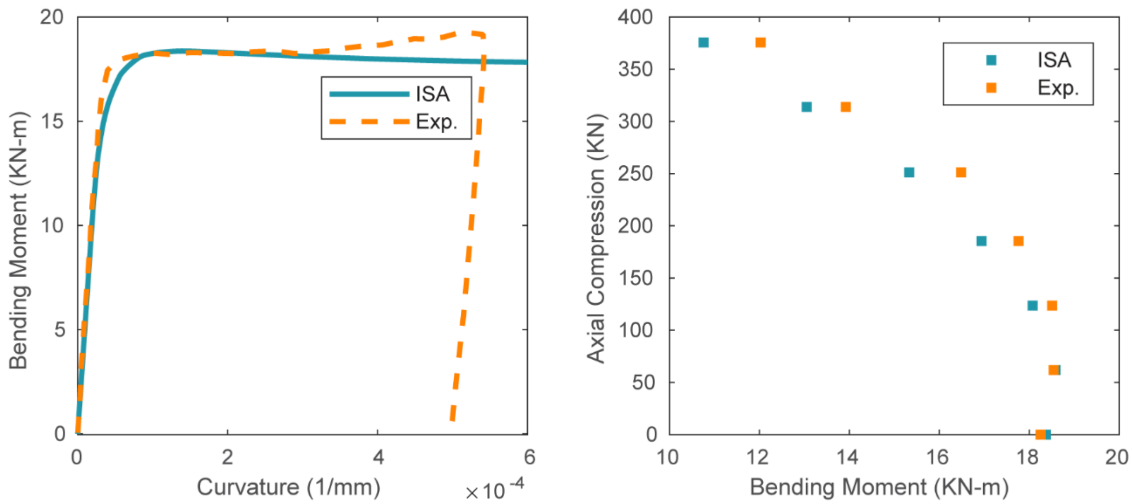

Figure 1-5. Example of the validation studies for the inelastic section analysis against experiments performed by Tomii and Sakino (1979) (a) moment-curvature response for specimen IV-0 (b) limit points for the IV series of specimens

100 mm, thickness of 4.25 mm, and yield stress of 285 MPa. The concrete had a compressive strength of 18.6 or 19.8 MPa. Figure 1-5a presents moment-curvature results for specimen IV-0 which was not subjected to axial load. Figure 1-5b presents limit point results for all 7 specimens in the series. Note that while the strength of composite columns is well-captured by the relatively simple constitutive relations used in this work, post-peak degradation can be overestimated, particularly for members with higher axial load. Denavit and Hajjar (2014) have presented more advanced models that better capture the post-peak behavior. These models were not used in this work since the focus is on strength.

Many inelastic analyses are performed to construct the interaction strength diagram. In each analysis, an axial compressive load is applied to the cross section then held constant. Then, bending moments are applied in a specific proportion based on the angle of loading, θ (as defined in Figure 1-3), until a peak is reached. The applied compressive load and bending moments at the peak are recorded as a single point on the interaction strength diagram. The process is repeated for different selected axial loads and angles of loading until the desired density of points is achieved. Note that, in this method, the location and orientation of the neutral axis at peak strength is determined through the nonlinear solution algorithm within OpenSees such that equilibrium is maintained. This is in contrast with the methods of computing the interaction diagram for the PSD and SC methods where the location and orientation of the neutral axis are selected and the resulting axial load and bending moments are computed based on equilibrium. Linear interpolation was used to obtain values between computed points on interaction diagrams.

The three-dimensional interaction strength diagram computed using inelastic analysis for the example RCFT cross section described in the previous section is shown in Figure 1-2c. One quadrant of two-dimensional slices of the interaction diagram at three different axial loads is shown in Figure 1-3 along with the results from the two design methods. For this cross section, the inelastic analysis results lie between the PSD and SC results with the PSD method giving greater strengths and the SC results giving lower strengths. The shapes of the three curves obtained from the PSD, SC, and ISA methods are similarly convex.

Parametric Study

Composite columns can exhibit a wide range of behavior based on steel ratio, material strengths, and other parameters. This section describes a parametric study undertaken to better understand the range of behavior. Suites of RCFT, CCFT, and SRC cross sections are defined and three-dimensional interaction diagrams are computed for each using the various design methods and inelastic analysis.

Cross Sections

The selected RCFT cross sections vary in aspect ratio (H/B), steel ratio ($\rho_s = A_s/A_g$), steel yield stress (F_y), and concrete compressive strength (f'_c) as described in

Table 1-1. The outside height of the steel tube was taken as constant (H = 305 mm) and the thickness of the steel tube was computed based on the steel ratio. Local buckling of the steel tube is not considered in any of the methods described above. Therefore, only cross sections that are considered compact by the AISC Specification (AISC 2016) were considered in this work. Specifically, any cross section that did not satisfy the inequality of Equation 1-2 was omitted.

$$\frac{H-3t}{t} \leq 2.26\sqrt{\frac{E}{F_y}} \qquad (1\text{-}2)$$

where, E is the modulus of elasticity of steel.

A total of 3,408 RCFT cross sections were investigated in this study. This number was derived as the product of the number of variations for each parameter [7 (aspect ratios) × 8 (steel ratios) × 9 (values of F_y) × 8 (values of f'_c)

Table 1-1. Variation of the parameters for the RCFT and CCFT cross sections

Parameter	Values
Cross section aspect ratio[1], *H*/*B*	1.0, 1.25, 1.5, 1.75, 2.0, 2.5, and 3.0
Steel ratio, ρ_s	0.08, 0.10– 0.40 (increments of 0.05)
Steel yield stress, F_y	240–520 MPa (increments of 35 MPa)
Concrete compressive strength, f'_c	20–69 MPa (increments of 7 MPa)

[1] Aspect ratio only varied for the RCFT cross sections

= 4,032] minus 624 cross sections that were omitted because they were not compact.

The selected CCFT cross sections vary in steel ratio (ρ_s), steel yield stress (F_y), and concrete compressive strength (f'_c) as described in Table 1-1. The outside diameter of the steel tube was taken as constant (D = 305 mm) and the thickness of the steel tube was computed based on the steel ratio. Only cross sections that are considered compact by the AISC *Specification* (AISC 2016) were considered in this work. Specifically, any cross section that did not satisfy the inequality of Equation 1-3 was omitted.

$$\frac{D}{t} \leq \frac{0.09E}{F_y} \tag{1-3}$$

A total of 520 CCFT cross sections were investigated in this study. This number was derived as the product of the number of variations for each parameter [8 (steel ratios) × 9 (values of F_y) × 8 (values of f'_c) = 576] minus 56 cross sections that were omitted because they were not compact.

The selected SRC cross sections vary in aspect ratio (H/B), steel shape, steel yield stress (F_y), concrete compressive strength (f'_c), reinforcing configuration, and reinforcing yield stress (F_{ysr}) as described in Table 1-2.

The gross area of the cross sections was taken as constant (A_g = 819,025 mm^2) so that the steel and reinforcing ratios would remain constant when changing the aspect ratio. The longitudinal reinforcing bars were placed in the cross sections symmetrically in the corners with a clear spacing equal to the greater of 38 mm or 1.5 times the diameter of the bar. For square cross sections, the number of bars along each face was equal. For cross sections with larger aspect ratios, the number of bars along the longer face was greater as described in Table 1-3. The notation for reinforcing configuration identifies the number of bars along the *x*- and *y*-axes of the cross section (Griffis 1992). For example, the reinforcing configuration is 4x-6y for the SRC cross section shown in Figure 1-1a. The bar spacing requirements could not be met in some cases. These cross sections were omitted from the study as described in the footnote to Table 1-4. A

Table 1-2. Various of the parameters for the SRC cross sections

Parameter	Values
Cross section aspect ratio, H/B	1.0, 1.25, 1.5, 1.75, and 2.0
Steel shape	W360×1299, W360×990, W360×677, W360×314, W360×262, W360×196, W360×134, and W250×73 (ρ_s = 0.198, 0.151, 0.103, 0.048, 0.040, 0.030, 0.020, and 0.011)
Steel yield stress, F_y	240–520 MPa (increments of 35 MPa)
Concrete compressive strength, f'_c	20–69 MPa (increments of 7 MPa)
Reinforcing configuration	12 #32, 20 #36, and 28 #36 (A_{sr}/A_g = 0.012, 0.024, and 0.034)
Reinforcing yield stress, F_{ysr}	280 MPa and 420 MPa

Table 1-3. Reinforcement configurations for SRC cross sections

Cross section aspect ratio	Reinforcing Configuration		
	12 #32	20 #36	28 #36
1.0	4x-4y	6x-6y	8x-8y
1.25	4x-4y	6x-6y	6x-10y
1.5	4x-4y	6x-6y [1]	6x-10y [1]
1.75	4x-4y	4x-8y [2]	6x-10y [2]
2.0	4x-4y [3]	4x-8y [3]	6x-10y [4]

[1] Not used with ρ_s = 0.198
[2] Not used with $\rho_s \geq 0.103$
[3] Not used with $\rho_s \geq 0.151$
[4] Not used with $\rho_s \geq 0.04$

clear cover of 38 mm was provided from the ties to the outside surface of the concrete. The size of the tie bars was based on the size of the longitudinal bars, #10 and #13 tie bars were used with #32 and #36 longitudinal bars, respectively. The tie spacing was assumed to be 305 mm.

A total of 14,688 SRC cross sections were investigated in this study. This number was derived as the product of the number of variations for each parameter [5 (aspect ratios) × 8 (steel shapes) × 9 (values of F_y) × 8 (values of f'_c) × 3 (reinforcing configurations) × 2 (values of F_{ysr}) = 17,280] minus 2,592 cross sections that were omitted because the spacing requirements could not be met.

Comparison of Methods

The different methods of calculating the interaction strength all yield somewhat different results. As a means of evaluating the methods, the interaction diagrams for each of the cross sections described in the preceding section and using each of the different methods (i.e., PSD, SC, and ISA) are computed and compared. For the RCFT and SRC cross sections, three-dimensional interaction diagrams were computed as a series of 9 two-dimensional interaction diagrams each with a given ratio of M_x to M_y. The angles of the interaction diagram (θ as defined in Figure 1-3) in M_x-M_y plane was equally spaced from 0 to π/2. Since all the selected cross sections are doubly symmetric, it was unnecessary to evaluate angles outside of this range. Only a single two-dimensional interaction diagram was computed for each of the CCFT cross sections since they are axisymmetric. Differences between any two interaction diagrams were computed as a function of angle in the M_θ-P plane using the radial measure defined in Equation 1-4, where M_θ is the resultant flexural moment strength in loading angle θ.

$$\varepsilon = \frac{r_1 - r_2}{r_1} \tag{1-4}$$

The results from the ISA are assumed to be the most accurate and the basis for evaluating the design methods. Thus, r_1 is taken as r_{ISA} and r_2 is taken as either r_{PSD} or r_{SC} where the radial distances are illustrated in Figure 1-6. Accordingly, positive values of ε indicate that the design method underpredicts the strength (i.e., conservative error).

A summary of the range of errors computed for the PSD method in comparison to the ISA method is presented in Table 1-4 for the RCFT cross sections,

Table 1-5 for the CCFT cross sections, and Table 1-6 for the SRC cross sections. The error was computed for all cross sections, all angles within the M_x-M_y plane, and in 1-degree increments in the M_θ-P plane where P is normalized by the pure axial strength from ISA and M_θ is normalized by the pure bending moment strength about the x-axis from ISA. The computed errors are then separated into bins based on steel ratio, steel yield strength, and loading region (i.e., high moment region, intermediate region, and high axial region as shown in Figure 1-6). The maximum, minimum, and average errors for each bin are shown in the tables.

The results show the potential for the PSD method to produce unconservative results. The greatest unconservative errors are seen for steel-dominant (higher steel ratio and/or higher steel yield stress) SRC cross sections with lower axial loads. The worst-case unconservative error is 38.6%, which occurs for y-axis bending (Table 1-6). The worst-case unconservative error in x-axis bending is 29.6%.

The errors for the filled composite members are not as significant. The greatest unconservative errors for the RCFT cross sections occur with higher steel yield stresses and a range of steel ratios and loading conditions. The worst-case unconservative error is 13.9% (Table 1-4). The maximum unconservative errors for x-axis bending, y-axis bending, and biaxial bending were similar for the RCFT cross sections. Unconservative errors were noted for the CCFT cross

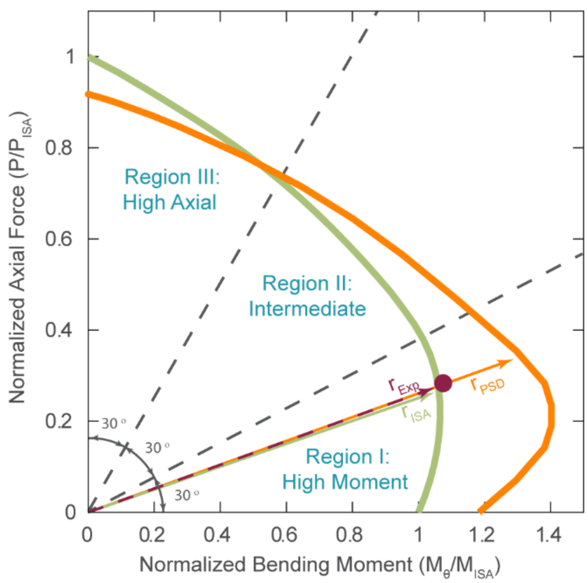

Figure 1-6. Computation of error for design methods

Table 1-4. Summary of error between PSD and ISA methods for RCFT cross sections

Yield Stress		F_y = 240, 275, 310 MPa			F_y = 345, 380, 415 MPa			F_y = 450, 485, 520 MPa		
Region		I	II	III	I	II	III	I	II	III
ρ_s = 0.08, 0.10	Max	2.4%	7.4%	11.5%	1.9%	3.3%	8.2%	1.3%	-0.6%	5.2%
	Avg.	-1.1%	0.3%	5.4%	-4.3%	-4.2%	1.2%	-7.0%	-8.2%	-2.4%
	Min	-5.4%	-5.4%	-2.9%	-10.4%	-10.4%	-8.6%	-13.5%	-13.5%	-12.0%
ρ_s = 0.15, 0.20	Max	4.7%	5.0%	9.8%	3.8%	2.1%	5.7%	3.5%	-1.4%	2.2%
	Avg.	-0.2%	-0.7%	3.6%	-2.4%	-3.9%	-0.1%	-4.1%	-6.9%	-3.4%
	Min	-4.7%	-5.1%	-3.5%	-9.0%	-9.2%	-6.8%	-13.7%	-13.9%	-10.2%
ρ_s = 0.25, 0.30	Max	7.6%	3.9%	9.0%	7.3%	2.9%	4.1%	7.3%	3.3%	3.4%
	Avg.	2.0%	0.5%	3.7%	0.5%	-1.9%	0.7%	-0.5%	-3.6%	-1.8%
	Min	-3.4%	-3.9%	-2.1%	-7.7%	-8.4%	-5.7%	-11.0%	-12.2%	-9.8%
ρ_s = 0.35, 0.40	Max	11.3%	7.3%	9.8%	11.2%	7.6%	7.9%	11.3%	8.0%	7.7%
	Avg.	4.8%	2.8%	5.1%	3.9%	1.2%	2.9%	3.5%	0.4%	1.3%
	Min	-1.2%	-2.0%	-0.6%	-4.0%	-5.4%	-4.1%	-5.5%	-7.5%	-6.9%

Table 1-5. Summary of error between PSD and ISA methods for CCFT cross sections

Yield Stress		F_y = 240, 275, 310 MPa			F_y = 345, 380, 415 MPa			F_y = 450, 485, 520 MPa		
Region		I	II	III	I	II	III	I	II	III
ρ_s = 0.08, 0.10	Max	11.3%	11.3%	13.5%	10.2%	11.8%	13.8%	10.3%	11.8%	13.8%
	Avg.	3.6%	4.9%	8.2%	4.4%	6.3%	9.4%	5.2%	7.6%	10.5%
	Min	-1.3%	-0.6%	3.2%	-1.1%	-0.7%	3.1%	1.5%	3.4%	6.4%
ρ_s = 0.15, 0.20	Max	19.1%	20.8%	21.0%	17.8%	19.8%	20.2%	16.6%	18.7%	19.5%
	Avg.	10.8%	13.6%	15.4%	10.7%	14.3%	16.0%	10.5%	14.5%	16.2%
	Min	4.5%	7.1%	9.7%	5.0%	8.6%	10.9%	5.4%	9.5%	11.7%
ρ_s = 0.25, 0.30	Max	20.9%	23.1%	24.9%	18.5%	20.7%	22.1%	17.2%	19.3%	20.3%
	Avg.	14.6%	18.3%	19.5%	13.5%	18.0%	19.2%	12.6%	17.4%	18.6%
	Min	9.9%	12.8%	15.1%	8.6%	14.0%	16.2%	7.7%	14.6%	16.7%
ρ_s = 0.35, 0.40	Max	20.8%	23.1%	25.4%	18.5%	20.8%	22.2%	17.2%	19.4%	20.4%
	Avg.	15.9%	20.3%	21.5%	14.0%	18.9%	20.1%	12.6%	17.5%	18.7%
	Min	10.8%	16.6%	18.3%	9.0%	15.2%	17.2%	7.5%	13.2%	15.0%

Table 1-6. Summary of error between PSD and ISA methods for SRC cross sections

Yield Stress		F_y = 240, 275, 310 MPa			F_y = 345, 380, 415 MPa			F_y = 450, 485, 520 MPa		
Region		I	II	III	I	II	III	I	II	III
ρ_s = 0.01, 0.02	Max	12.4%	11.9%	14.2%	9.1%	11.5%	14.0%	6.7%	10.6%	13.7%
	Avg.	1.1%	6.0%	10.6%	-0.6%	4.4%	9.7%	-2.6%	2.1%	8.0%
	Min	-6.3%	-2.7%	4.1%	-10.3%	-6.8%	1.1%	-15.8%	-11.4%	-4.2%
ρ_s = 0.03, 0.04	Max	6.0%	10.1%	13.4%	4.8%	8.9%	12.9%	4.0%	6.9%	12.3%
	Avg.	-0.9%	4.0%	9.2%	-4.0%	1.3%	7.7%	-7.7%	-2.3%	4.7%
	Min	-9.0%	-6.9%	2.2%	-16.2%	-12.7%	-3.3%	-23.9%	-20.2%	-9.4%
ρ_s = 0.05, 0.10	Max	4.9%	8.5%	12.7%	3.8%	7.0%	11.9%	3.0%	4.3%	11.2%
	Avg.	-3.3%	1.3%	7.1%	-7.9%	-2.3%	5.1%	-12.9%	-6.9%	1.4%
	Min	-16.1%	-13.7%	-3.0%	-24.8%	-22.2%	-6.8%	-33.8%	-30.0%	-12.2%
ρ_s = 0.15, 0.20	Max	2.4%	4.2%	9.3%	1.0%	1.4%	8.0%	-0.2%	-1.9%	7.0%
	Avg.	-6.4%	-2.9%	3.6%	-11.6%	-7.3%	1.3%	-15.7%	-11.6%	-2.4%
	Min	-18.3%	-16.9%	-3.5%	-28.5%	-25.9%	-7.9%	-38.6%	-35.1%	-14.0%

sections with lower steel ratios. However, the worst-case unconservative error is 1.3% (Table 1-5), indicating that the PSD method produces a safe evaluation of CCFT cross section strength over the range of parameters considered in this study.

A summary of the range of errors computed for the SC method is presented in Table 1-7 for the RCFT cross sections and Table 1-8 for the SRC cross sections. The SC method was not evaluated for the CCFT cross sections because the PSD method was found to be sufficiently safe. These tables were prepared in the same manner as Table 1-4 through Table 1-6. In contrast to the PSD method, only fairly minor unconservative errors are noted for the SC method. The maximum unconservative error for all the SRC cross sections studied is just over 1%. For the RCFT cross sections, the maximum unconservative error is less than 5%. However, the conservative errors are significantly higher than with the PSD method, with a maximum conservative error of 32% for the RCFT cross sections and 50% for the SRC cross sections. Comparing the two design methodologies against each other, the SC method provides lower strengths than the PSD method in all cases. This is expected since, for a given neutral axis location, the assumed stress for the SC method is always less than or equal to the assumed stress for the PSD method. The differences between the methods increase with increases in steel yield strength and steel ratio. Utilizing Equation 1-4 with $r_1 = r_{PSD}$ and $r_2 = r_{SC}$, the maximum error, ε, is 40% for RCFT cross sections and 110% for SRC cross section. Limiting the results to uniaxial bending (i.e., $\theta = 0$ or $\pi/2$) the maximum errors reduce to 20% for RCFT cross sections and 70% for SRC cross sections.

Modified Plastic Stress Distribution (MPSD) Method

As identified in the previous section, the PSD method can yield unconservative results, especially for SRC cross sections with high steel ratios and high steel yield strengths. At the same time, the SC method was found to be

Table 1-7. Summary of error between SC and ISA methods for RCFT cross sections

Yield Stress		F_y = 240, 275, 310 MPa			F_y = 345, 380, 415 MPa			F_y = 450, 485, 520 MPa		
Region		I	II	III	I	II	III	I	II	III
ρ_s = 0.08, 0.10	Max	13.3%	13.1%	24.8%	16.2%	13.5%	21.9%	22.1%	20.3%	19.4%
	Avg.	6.4%	6.3%	13.9%	7.6%	5.1%	9.7%	11.0%	6.0%	6.9%
	Min	0.2%	1.6%	1.5%	-1.6%	-1.4%	-2.3%	-2.2%	-2.3%	-4.3%
ρ_s = 0.15, 0.20	Max	13.3%	13.0%	23.3%	18.4%	17.6%	19.9%	27.1%	26.1%	16.9%
	Avg.	7.4%	6.8%	11.0%	9.7%	7.0%	7.7%	14.1%	9.1%	5.9%
	Min	1.5%	2.2%	1.6%	1.2%	1.2%	0.3%	2.4%	-0.2%	-1.3%
ρ_s = 0.25, 0.30	Max	14.3%	13.9%	22.6%	21.4%	20.8%	18.5%	29.6%	28.8%	18.5%
	Avg.	9.1%	8.1%	10.8%	11.9%	9.2%	8.4%	16.6%	12.3%	7.6%
	Min	3.0%	3.3%	3.0%	3.3%	2.7%	1.1%	3.7%	1.1%	-0.3%
ρ_s = 0.35, 0.40	Max	17.1%	16.8%	23.3%	23.8%	23.3%	21.7%	31.7%	31.0%	21.6%
	Avg.	11.1%	10.1%	12.1%	14.2%	11.9%	10.5%	19.0%	15.4%	10.6%
	Min	4.7%	4.9%	4.6%	5.0%	4.3%	2.8%	5.3%	3.5%	1.8%

Table 1-8. Summary of error between SC and ISA methods for SRC cross sections

Yield Stress		F_y = 240, 275, 310 MPa			F_y = 345, 380, 415 MPa			F_y = 450, 485, 520 MPa		
Region		I	II	III	I	II	III	I	II	III
ρ_s = 0.01, 0.02	Max	20.9%	21.9%	27.1%	22.9%	21.9%	26.9%	25.3%	23.3%	26.7%
	Avg.	10.6%	10.8%	20.6%	11.5%	10.6%	19.8%	12.4%	10.6%	18.5%
	Min	2.1%	6.1%	7.5%	2.2%	6.0%	7.2%	2.0%	6.2%	7.6%
ρ_s = 0.03, 0.04	Max	22.6%	20.9%	26.4%	25.8%	24.4%	26.0%	28.6%	27.2%	25.4%
	Avg.	11.7%	9.3%	19.0%	13.6%	9.5%	17.9%	15.4%	10.9%	16.3%
	Min	1.4%	4.8%	6.6%	3.4%	4.7%	5.8%	4.4%	4.8%	6.3%
ρ_s = 0.05, 0.10	Max	25.9%	23.7%	25.8%	33.5%	31.1%	25.1%	40.5%	38.4%	28.9%
	Avg.	13.3%	8.3%	16.9%	16.9%	9.6%	15.6%	20.4%	13.1%	14.8%
	Min	2.4%	3.0%	3.7%	4.1%	1.8%	2.2%	5.0%	2.1%	2.3%
ρ_s = 0.15, 0.20	Max	28.4%	27.1%	22.9%	39.4%	37.4%	21.9%	50.1%	48.0%	34.2%
	Avg.	15.0%	7.9%	13.2%	22.4%	11.5%	12.4%	30.3%	19.2%	13.7%
	Min	2.0%	1.6%	2.0%	4.0%	0.4%	0.5%	7.1%	1.0%	1.0%

conservative, but overly so in many cases. Both of these methods have an advantage of simplicity and ease of use over the ISA method. In this section, the cause of the unconservative error in the PSD method is investigated and a modification is proposed such that more accurate results can be obtained within the existing framework of the PSD method.

To better understand the cause of the unconservative error in the PSD method, one SRC cross section is analyzed using the PSD, SC, and ISA methods with the contributions of the structural steel and reinforced concrete (RC) components tracked separately. The SRC cross section is square with H=B=700 mm, steel shape of W310×500 (ρ_s = 0.13), 12 #10 bars in a 4x-4y configuration (A_{sr}/A_g = 0.02), F_y = 517 MPa, F_{ysr} = 414 MPa, and f'_c = 55 MPa. For this cross section and y-axis bending, the maximum unconservative error with respect to the ISA is 26% for the PSD method. No unconservative error is found for this cross section with the SC method.

Moment-curvature results for this cross section from the ISA at a constant axial compression of $0.5P_{no}$ are shown in Figure 1-7. The total moment within the composite cross section is shown along with the portions resisted by the structural steel and reinforced concrete components of the cross section. Additionally, the total moment strength and portions of strength from each component from the PSD method are shown as horizontal lines. The peak moment from the ISA occurs relatively early in the analysis, shortly after the reinforced concrete attains its peak moment. The peak moment in the reinforced concrete is similar to that predicted by the PSD method. However, the structural steel shape has not fully yielded when the concrete has reached its peak, meaning that it cannot contribute to the strength in the amount assumed by the PSD method, resulting in an overprediction of strength by the PSD method. The PSD method relies on the assumption that plastic strengths of both the structural steel and reinforced concrete components occur simultaneously. The results of

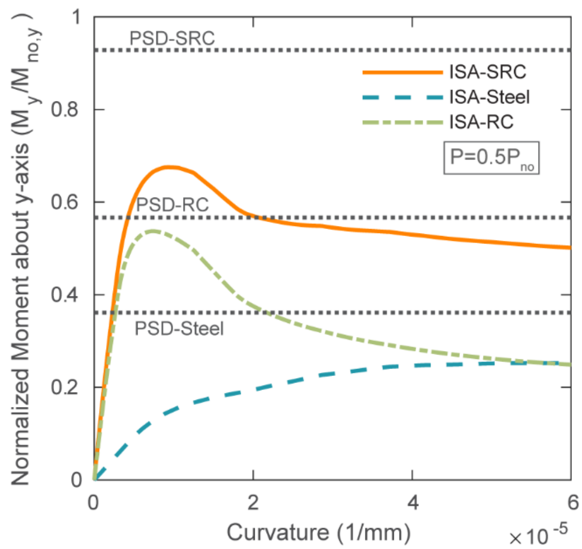

Figure 1-7. Moment curvature diagram for each portion of example SRC cross section

Figure 1-7 show that this is clearly not the case. It is also interesting that the moment in the steel shape does not approach the moment obtained from the PSD method. This is caused by the fact that the axial load within the steel shape also differs from that obtained from the PSD method.

Interaction diagrams for the example SRC cross section are shown in Figure 1-8. Again, the total moment is shown along with the moment in each of the two components of the cross section. From this figure, it is clear that for this cross section the unconservative error in the PSD method is caused by overestimation of the contribution from the steel shape for all but the highest axial loads ($P \leq 0.7P_{no}$). The SC method, on the other hand, captures the shape of the contribution of the steel shape more accurately, but underestimates the magnitude.

Modification Factor

Modifications to the PSD method to achieve more accurate results can take many forms. Some focus on the assumed stress distributions. Chen (2012) presents a modification where the rectangular stress block described in the ACI Code (ACI 2019) is used instead of extending the stress block to the neutral axis. This method brings greater consistency between the PSD and SC methods and reduces some error, but does little to correct the largest unconservative errors noted in this work mainly caused by an overestimation of the contribution of the steel shape. Modifications that focus on steel stress may prove to be more effective. However, a different sort of modification is derived in this work.

The proposed modification leaves the assumed stresses of the PSD method unchanged and simply reduces the strength by applying a factor to the results. Figure 1-9 shows the ratio of moment obtained from the ISA method, M_{ISA}, to the moment obtained from the PSD method, M_{PSD}, for the example SRC cross section. From these results, a modification factor that is a linear function of

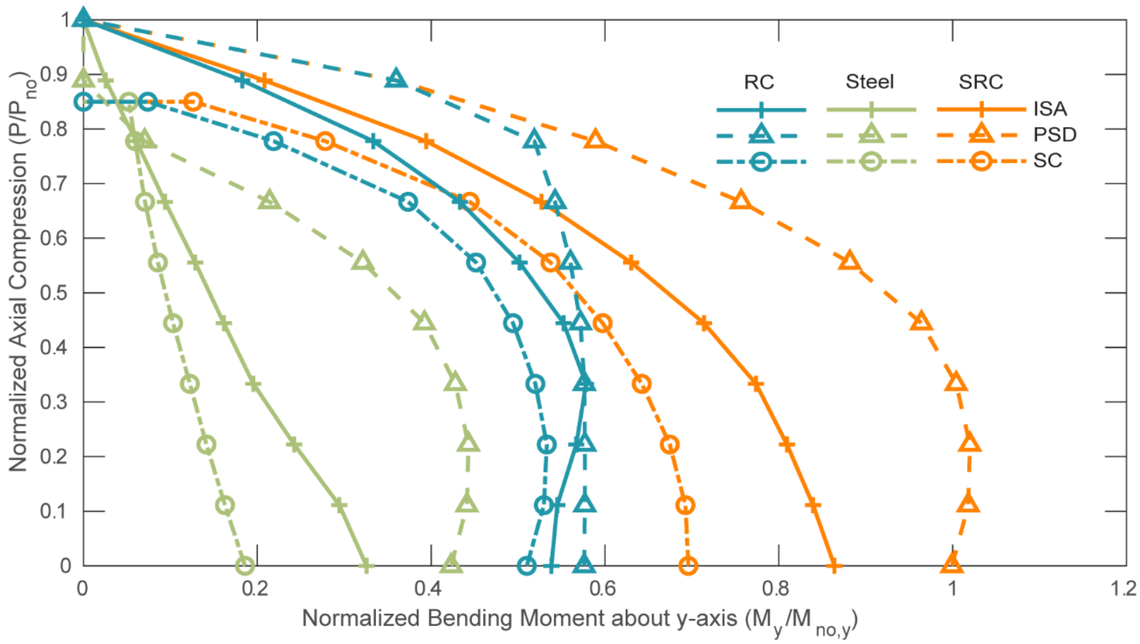

Figure 1-8. Two-dimensional strength interaction diagrams for example SRC cross section showing component contributions

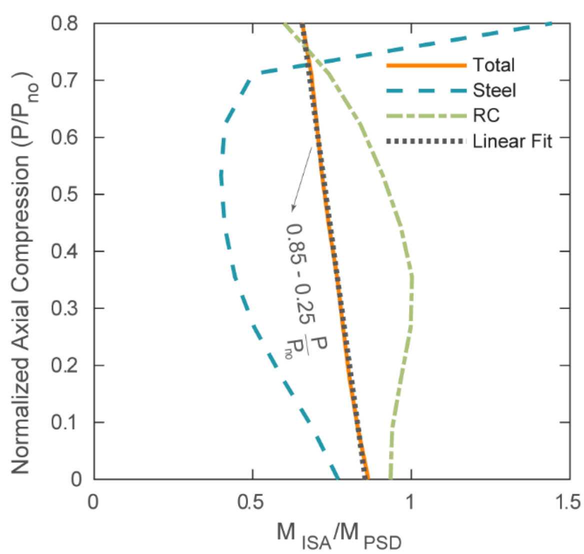

Figure 1-9. Comparison of ISA and PSD results for example SRC cross section

the axial compression appears to be a good candidate in reducing the error between the two. An examination of results from the other cross sections from the parametric study indicates that a linear function of axial compression is indeed suitable for a wide range of cross sections, however, the coefficients of the linear function vary significantly. Such a modification factor could be defined by Equation 1-5.

$$\psi = \varphi_1 - \varphi_2\left(\frac{P}{P_{no}}\right) \le 1.0 \qquad (1\text{-}5)$$

where, φ_1 and φ_2 are calibrated parameters selected to achieve optimal results and "≤ 1.0" indicates that if the calculated result is greater than 1.0, then ψ should be taken as 1.0.

When φ_1 and φ_2 are individually computed with linear regression for each of the parametric set of cross sections (e.g., as shown in Figure 1-9), it is observed that they both are correlated to the steel strength ratio (A_sF_y/P_{no}). In order to derive a relationship for φ_1 and φ_2, an optimization problem is designed in which two linear equations representing φ_1 and φ_2 as functions of A_sF_y/P_{no} are assumed, and the parameters of these two equations are selected in a way that the unconservative error of the MPSD method compared to the ISA method for the entire parametric suite of cross sections is minimized. For this purpose, an objective function was defined with four inputs (two parameters for the φ_1 equation and two parameters for the φ_2 equation) and one output, the summation of the absolute value of the total conservative (positive) and unconservative (negative) errors for the MPSD method with respect to the ISA method for the parametric suite of cross sections. In other words, the MPSD interaction strength should be close to the ISA interaction strength to reduce the amount of error. The optimization problem was run separately for SRC and RCFT cross sections given the difference in magnitude of error observed. Since the distribution of φ_1 and φ_2 are observed to be quite similar for bending about the *x*- and *y*-axes, and for the sake of simplicity, the data from both axes were used to derive the φ_1 and φ_2 equations. To solve the global optimization problem, a multi-point search tool and the nonlinear multi-variable optimizer were used (Dixon 1978; Ugray et al. 2007). The optimum equations for φ_1 and φ_2 are presented in Equations 1-6 and 1-7 for SRC and RCFT cross sections respectively.

$$\varphi_1 = 1.0 - 0.15\frac{A_s F_y}{P_{no}} \quad (\mathrm{SRC}) \tag{1-6a}$$

$$\varphi_2 = -0.15 + 0.75\frac{A_s F_y}{P_{no}} \quad (\mathrm{SRC}) \tag{1-6b}$$

$$\varphi_1 = 1.0 + 0.05\frac{A_s F_y}{P_{no}} \quad (\mathrm{RCFT}) \tag{1-7a}$$

$$\varphi_2 = 0.10 + 0.15\frac{A_s F_y}{P_{no}} \quad (\mathrm{RCFT}) \tag{1-7b}$$

Comparison of Methods

Figure 1-10 presents a histogram of the maximum unconservative and maximum conservative errors for each cross section in the parametric suite and both the PSD and MPSD methods. For the SRC cross sections, the maximum unconservative error is reduced from 38% to 12% (Figure 1-10a). The 95th percentile of unconservative error is reduced from 20% to less than 5%. The 95th percentile of conservative error is increased somewhat from 7% to 12% (Figure 1-10b). For the RCFT cross sections, the maximum unconservative error is reduced from 14% to 10% (Figure 1-10c). The 95th percentile of unconservative error is reduced from 10% to 5%. The 95th percentile of conservative error remained constant in the MPSD compared to the PSD method at about 8% (Figure 1-10d). These results highlight the efficiency of the proposed modification which effectively targets the cross sections where the unconservative error is expected while minimizing unnecessary reductions. This is especially true for

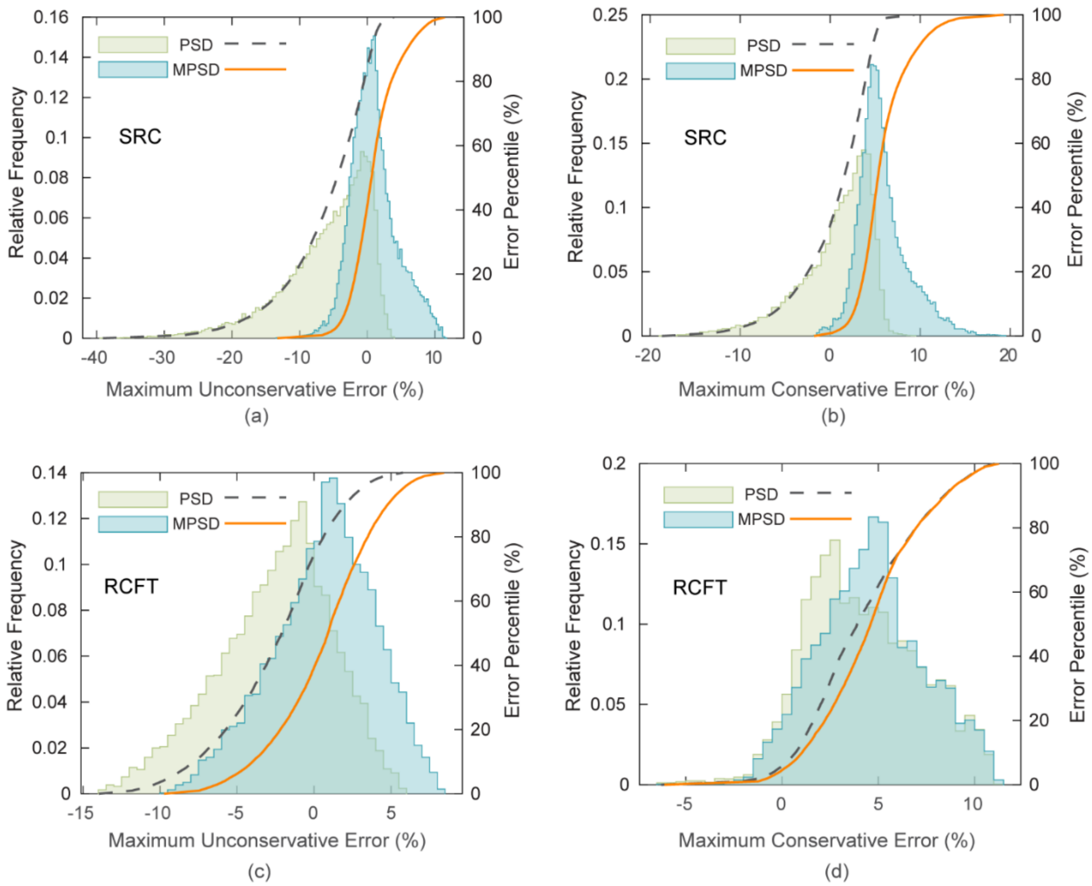

Figure 1-10. Histograms of error in benchmark cross sections (a) maximum unconservative error for SRC cross sections (b) maximum conservative error for SRC cross sections (c) maximum unconservative error for RCFT cross sections (d) maximum conservative error for RCFT cross sections

SRC cross sections. For the RCFT cross sections, the potential errors with the PSD method are less critical than for the SRC cross sections and the reduction in error from using the MPSD method is more modest. Accordingly, the use of the PSD method, without modification, may be deemed appropriate for design.

Experimental Validation

Hundreds of experimental tests have been performed on encased composite members (Kim 2005). The results of some of these tests can be used to further evaluate the current design methods as well as the proposed modification. In particular, two studies that included tests on short SRC beam-columns have been identified for this comparison (Virdi and Dowling 1973; Morino et al. 1984a). In this work, short columns were defined as those having a length to width ratio less than 8. With this ratio, the member axial compressive strength computed in accordance with the AISC Specification (2016) was no more than 10% lower than the cross section axial compressive strength. Morino et al. (1984a) investigated the ultimate strength of 40 SRC beam-columns under a combination of axial compression and uniaxial or biaxial bending. These tests included 10 short column specimens with various eccentricities. Virdi and Dowling (1973) performed an experimental study on the behavior and strength of SRC columns subjected to biaxially eccentric compression load. These tests included a series of nine encased composite specimens with various lengths and biaxial eccentricities, in which 3 specimens were considered as short columns. Experimental tests of short encased composite beam-columns described in other works have not been included in this comparison because the concrete encasement was not reinforced or because the load was applied cyclically.

In total, 13 SRC specimens were identified for this comparison. Details of the specimens are presented in Table 1-9. For each specimen, four different three-dimensional interaction surfaces were computed using each of the SC, ISA, PSD, and MPSD methods. The ratio of the radial distance from the origin to

Table 1-9. Properties of SRC experimental specimens

Index	Specimen Label	Steel Shape	H, B (mm)	F_y (MPa)	f'_c (MPa)	d_b (mm)	F_{ysr} (MPa)	L (mm)	Reference
1	A4-0	H100X100X6X8	160	345	21.1	6.35	414	960	Morino et al. (1984)
2	A4-30	H100X100X6X8	160	345	21.1	6.35	414	960	Morino et al. (1984)
3	A4-45	H100X100X6X8	160	345	21.1	6.35	414	960	Morino et al. (1984)
4	A4-60	H100X100X6X8	160	345	21.1	6.35	414	960	Morino et al. (1984)
5	A4-90	H100X100X6X8	160	345	21.1	6.35	414	960	Morino et al. (1984)
6	A8-0	H100X100X6X8	160	345	33.6	6.35	414	960	Morino et al. (1984)
7	A8-30	H100X100X6X8	160	345	33.6	6.35	414	960	Morino et al. (1984)
8	A8-45	H100X100X6X8	160	345	33.6	6.35	414	960	Morino et al. (1984)
9	A8-60	H100X100X6X8	160	345	33.6	6.35	414	960	Morino et al. (1984)
10	A8-90	H100X100X6X8	160	345	33.6	6.35	414	960	Morino et al. (1984)
11	A	W150X22.5	254	315	39.6	12.7	309	1857	Virdi and Dowling (1973)
12	B	W150X22.5	254	315	37.9	12.7	309	1857	Virdi and Dowling (1973)
13	C	W150X22.5	254	315	39.6	12.7	309	1857	Virdi and Dowling (1973)

the experimental data point and from the origin to each interaction surface (along the same line as to the experimental data point) was calculated. An example interaction diagram for one specimen (specimen No. 9 from Table 1-9) is shown in Figure 1-6. The computed test-to-predicted ratios for all specimens are presented in Table 1-10.

The ISA and MPSD methods are the most precise with average test-to-predicted ratios of 0.98 and 0.99 respectively. However, the ISA method is more precise with a standard deviation of the test-to-predicted ratios of 0.07, in contrast to 0.10 for the MPSD method. The SC method is seen to underpredict the strength with an average test-to-predicted ratio of 1.09 and the PSD method is seen to overpredict the strength with an average test-to-predicted ratio of 0.87. These results correspond well with the results of the parametric study where the SC was found to be generally conservative, the PSD method was found to be capable of resulting in unconservative error, and the MPSD method being calibrated based on the results from the ISA method.

Conclusions

The plastic stress distribution (PSD) method is commonly used for calculating the strength of steel concrete composite column cross sections. While the accuracy of this method has been evaluated for some cases, no previous study has systematically evaluated its accuracy over the whole range of materials, cross-sectional geometries, and loading conditions for which it is permitted to be applied.

In this work, a broad parametric study was performed to assess the strength of steel-concrete composite cross sections subjected to axial compression and uniaxial/biaxial bending to evaluate these approaches to compute the interaction strength. For this purpose, three-dimensional strength interaction diagrams were computed for a parametric suite of thousands of composite cross sections using the PSD and SC methods as well as with a fiber-based inelastic section analysis.

Table 1-10. Results of comparison for SRC experimental specimens

Index	P (kN)	M_x (kN-m)	M_y (kN-m)	Expt. vs. SC	Expt. vs. ISA	Expt. vs. PSD	Expt. vs. MPSD
1	499.71	0.00	19.99	1.07	1.00	0.84	1.02
2	513.24	10.26	17.78	1.11	0.97	0.81	0.99
3	518.62	14.67	14.67	1.03	0.91	0.78	0.92
4	524.04	18.15	10.48	0.94	0.86	0.78	0.91
5	740.14	29.61	0.00	1.18	1.15	1.11	1.27
6	344.20	0.00	25.82	1.00	0.93	0.84	0.97
7	376.90	14.13	24.48	1.14	0.99	0.85	0.98
8	378.63	20.08	20.08	1.06	0.94	0.75	0.85
9	447.49	29.07	16.78	1.11	1.01	0.82	0.93
10	520.62	39.05	0.00	1.05	1.00	0.93	1.06
11	1256.02	46.26	79.76	1.04	0.93	0.88	0.94
12	647.95	47.73	82.29	1.13	0.98	0.92	0.99
13	473.50	52.32	90.20	1.26	1.09	1.03	1.09
Average				1.09	0.98	0.87	0.99
Standard Deviation				0.08	0.07	0.10	0.10

In comparison to the ISA method, the SC method was found to be conservative, predicting lower strengths in almost all cases. The PSD method, on the other hand, was found to produce unconservative errors for some cross sections. For SRC cross sections, this error was greatest with high steel ratios and high steel yield stresses, with unconservative error as much as 38% in *y*-axis bending and 29% in *x*-axis bending. For RCFT cross sections, the maximum unconservative error was found to be about 14% which occurred for cross sections with high steel yield stress. For CCFT cross sections, the maximum unconservative error was found to be about 1%. A simple modification to the PSD method was proposed to reduce the unconservative error in SRC and RCFT cross sections. This modification was calibrated based on inelastic section analysis results. With the modification, the 95th percentile of unconservative error in the broad range of cross sections examined was reduced to less than 5%, while the maximum conservative error increased slightly.

Validation against published experimental results confirmed that the PSD method overestimates the strength for some cross sections and that the MPSD method provides improved accuracy.

References

Abdel-Rahman, N., and Sivakumaran, K. S. (1997). "Material properties models for analysis of cold-formed steel members." *Journal of Structural Engineering*, 123, 1135–1143.

ACI. (2014). *Building Code Requirements for Structural Concrete and Commentary*. American Concrete Institute, Farmington Hills, MI.

ACI. (2018). *Report on Equivalent Rectangular Concrete Stress Block and Transverse Reinforcement for High-Strength Concrete Columns*. 441.1R-18, ACI.

ACI. (2019). *Building Code Requirements for Structural Concrete and Commentary*. American Concrete Institute, Farmington Hills, MI.

AISC. (1986). *Load and Resistance Factor Design Specification for Structural Steel Buildings*. American Institute of Steel Construction, Chicago, Illinois.

AISC. (2005). *Specification for Structural Steel Buildings*. American Institute of Steel Construction, Chicago, Illinois.

AISC. (2016). *Specification for structural steel buildings*. American Institute of Steel Construction, Chicago, Illinois.

AISC. (2017). *Steel Construction Manual, 15th Edition*. American Institute of Steel Construction, Chicago, Illinois.

ASCE. (1997). *Effective Length and Notional Load Approaches for Assessing Frame Stability: Implications for American Steel Design*. American Society of Civil Engineers, Reston, Virginia.

ASTM A6. (2019). *ASTM A6/A6M-11: Standard Specification for General Requirements for Rolled Structural Steel Bars, Plates, Shapes and Sheet Piling*. ASTM International West Conshohocken, PA.

ASTM A500. (2020). *ASTM A500/A500M: Standard Specification for Cold-Formed Welded and Seamless Carbon Steel Structural Tubing in Rounds and Shapes*. ASTM International West Conshohocken, PA.

ASTM A615. (2020). *ASTM A615/A615M: Standard Specification for Deformed and Plain Carbon-Steel Bars for Concrete Reinforcement*. ASTM International West Conshohocken, PA.

Behnam, A., and Denavit, M. D. (2020). "Plastic stress distribution method for predicting interaction strength of steel-concrete composite cross sections." *Journal of Constructional Steel Research*, 170, 106092.

Brent, R. P. (2013). *Algorithms for minimization without derivatives*. Courier Corporation.

Bridge, R. Q. (1976). *Concrete filled steel tubular columns*. School of Civil Engineering, University of Sydney, Sydney, Australia.

CEN. (2004). *Eurocode 4: Design of composite steel and concrete structures—Part 1.1: General rules and rules for buildings*. European Committee for Standardization, Brussels, Belgium.

Chen, C.-C. (2012). “Accuracy of AISC methods in predicting flexural strength of concrete-encased members.” *Journal of Structural Engineering*, 139(3), 338–349.

Denavit, M. D., and Hajjar, J. F. (2014). *Characterization of Behavior of Steel-Concrete Composite Members and Frames with Applications for Design*. Newmark Structural Laboratory Report Series, Newmark Structural Laboratory Report NSEL-034, University of Illinois at Urbana-Champaign, Urbana, Illinois.

Denavit, M. D., Hajjar, J. F., Perea, T., and Leon, R. T. (2016a). “Stability Analysis and Design of Composite Structures.” *Journal of Structural Engineering*, ASCE, 142(3), 04015157.

Denavit, M. D., Hajjar, J. F., Perea, T., and Leon, R. T. (2016b). “Stability analysis and design of composite structures.” *Journal of Structural Engineering*, 142, 1–12.

Dixon, L. C. W. (1978). “The global optimization problem. an introduction.” *Toward global optimization*, 2, 1–15.

Forsythe, G. E., Malcolm, M. A., and Moler, C. B. (1977). *Computer Methods for Mathematical Computations*. Prentice Hall.

Fujikura, S., Bruneau, M., and Lopez-Garcia, D. (2008). “Experimental investigation of multihazard resistant bridge piers having concrete-filled steel tube under blast loading.” *Journal of Bridge Engineering*, 13, 586–594.

Furlong, R. W., Hsu, C.-T. T., and Mirza, S. A. (2004). “Analysis and design of concrete columns for biaxial bending-overview.” *Structural Journal*, 101(3), 413–422.

Galambos, T. V., and Ketter, R. L. (1959). “Columns under combined bending and thrust.” *Journal of the Engineering Mechanics Division*, 85(2), 1–30.

Goode, C. D. (2008a). “Composite Columns - 1819 Tests on Concrete-Filled Steel Tube Columns Compared with Eurocode 4.” *The Structural Engineer*, 86(16), 33–38.

Goode, C. D. (2008b). “Composite columns-1819 tests on concrete-filled steel tube columns compared with Eurocode 4.” *The Structural Engineer*, 86, 33–38.

Gourley, B. C., Tort, C., Denavit, M. D., Schiller, P. H., and Hajjar, J. F. (2008a). *A synopsis of studies of the monotonic and cyclic behavior of concrete-filled steel tube members, connections, and frames*. Newmark Structural Engineering Laboratory. University of Illinois at Urbana-Champaign.

Gourley, B. C., Tort, C., Denavit, M. D., Schiller, P. H., and Hajjar, J. F. (2008b). *A Synopsis of Studies of the Monotonic and Cyclic Behavior of Concrete-Filled Steel Tube Members, Connections, and Frames*. Newmark Structural Laboratory Report NSEL-008, Department of Civil and Environmental Engineering, University of Illinois at Urbana-Champaign, Urbana, Illinois.

Griffis, L. G. (1992). *Load and Resistance Factor Design of W-Shapes Encased in Concrete*. Design Guide 6, American Institute of Steel Construction, Chicago, Illinois.

Hardika, M. S., and Gardner, N. J. (2004). "Behavior of concrete-filled hollow structural section beam columns to seismic shear displacements." *Structural Journal*, 101, 39–46.

Hatzigeorgiou, G. D. (2008). "Numerical model for the behavior and capacity of circular CFT columns, Part I: Theory." *Engineering Structures*, 30(6), 1573–1578.

Kanchanalai, T. (1977). *The Design and Behavior of Beam-Columns in Unbraced Steel Frames*. CESRL Report No. 77-2, Structures Research Laboratory, Department of Civil Engineering, The University of Texas at Austin, Austin, Texas.

Kim, D. K. (2005). "A Database for Composite Columns." M.S. Thesis, School of Civil and Environmental Engineering, Georgia Institute of Technology, Atlanta, Georgia.

Kostic, S. M., and Filippou, F. C. (2012). "Section discretization of fiber beam-column elements for cyclic inelastic response." *Journal of Structural Engineering*, American Society of Civil Engineers, 138(5), 592–601.

Lai, Z., and Varma, A. H. (2015). "Noncompact and slender circular CFT members: Experimental database, analysis, and design." *Journal of Constructional Steel Research*, 106, 220–233.

Lai, Z., and Varma, A. H. (2016). "Effective stress-strain relationships for analysis of noncompact and slender filled composite (CFT) members." *Engineering Structures*, Elsevier, 124, 457–472.

Lai, Z., Varma, A. H., and Zhang, K. (2014). "Noncompact and slender rectangular CFT members: Experimental database, analysis, and design." *Journal of Constructional Steel Research*, 101, 455–468.

Leon, R. T., Kim, D. K., and Hajjar, J. F. (2007). "Limit State Response of Composite Columns and Beam-Columns Part 1: Formulation of Design Provisions for the 2005 AISC Specification." *Engineering Journal*, AISC, 44(4), 341–358.

Liang, Q. Q. (2008). "Nonlinear analysis of short concrete-filled steel tubular beam–columns under axial load and biaxial bending." *Journal of Constructional Steel Research*, 64(3), 295–304.

Liang, Q. Q., Patel, V. I., and Hadi, M. N. (2012). "Biaxially loaded high-strength concrete-filled steel tubular slender beam-columns, Part I: Multiscale simulation." *Journal of Constructional Steel Research*, 75, 64–71.

MacGregor, J. G., and Hage, S. E. (1977). "Stability Analysis and Design of Concrete Frames." *Journal of the Structural Division, ASCE*, 103(10), 1953–1970.

McKenna, F., Scott, M. H., and Fenves, G. L. (2010a). "Nonlinear finite-element analysis software architecture using object composition." *Journal of Computing in Civil Engineering*, 24(1), 95–107.

McKenna, F., Scott, M. H., and Fenves, G. L. (2010b). "Nonlinear Finite-Element Analysis Software Architecture Using Object Composition." *Journal of Computing in Civil Engineering*, ASCE, 24(1), 95–107.

Morino, S., Matsui, C., and Watanabe, H. (1984a). “Strength of biaxially loaded SRC columns.” 185–194.

Morino, S., Matsui, C., and Watanabe, H. (1984b). “Strength of Biaxially Loaded SRC Columns.” *Composite and Mixed Construction*, American Society of Civil Engineers, 185–194.

Patel, V. I., Liang, Q. Q., and Hadi, M. N. (2015). “Biaxially loaded high-strength concrete-filled steel tubular slender beam-columns, Part II: Parametric study.” *Journal of Constructional Steel Research*, 110, 200–207.

Perea, T., Leon, R. T., Hajjar, J. F., and Denavit, M. D. (2014). “Full-scale tests of slender concrete-filled tubes: Interaction behavior.” *Journal of Structural Engineering*, 140, 04014054.

Ricles, J. M., and Paboojian, S. D. (1994). “Seismic performance of steel-encased composite columns.” *Journal of Structural Engineering*, 120, 2474–2494.

SAC. (2014). *Technical code for concrete filled steel tubular structures, GB 50936-2014*. Standardization Administration of the People’s Republic of China, Beijing.

Sakino, K., Nakahara, H., Morino, S., and Nishiyama, I. (2004). “Behavior of centrally loaded concrete-filled steel-tube short columns.” *Journal of Structural Engineering*, 130, 180–188.

Sanz Picon, C. F. (1992). “Behavior of composite column cross sections under biaxial bending.” MS.c. Thesis, Cornell University, Ithaca, New York.

Shakir-Khalil, H., and Mouli, M. (1990). “Further Tests on Concrete-Filled Rectangular Hollow-section columns.” *The Structural Engineer*, 68, 9.

Shakir-Khalil, H., and Zeghiche, J. (1989). “Experimental Behaviour of Concrete-Filled Rolled Rectangular Hollow-Section Columns.” *The Structural Engineer*, 67, 346–354.

Surovek-Maleck, A. E., and White, D. W. (2004). “Alternative approaches for elastic analysis and design of steel frames. I: Overview.” *Journal of Structural Engineering*, 130, 1186–1196.

Tokgoz, S., and Dundar, C. (2008). “Experimental tests on biaxially loaded concrete-encased composite columns.” *Steel and Composite Structures*, 8(5), 423–438.

Tomii, M., and Sakino, K. (1979). “Experimental studies on the ultimate moment of concrete filled square steel tubular beam-columns.” *Transactions of the Architectural Institute of Japan*, 275, 55–65.

Ugray, Z., Lasdon, L., Plummer, J., Glover, F., Kelly, J., and Martí, R. (2007). “Scatter search and local NLP solvers: A multistart framework for global optimization.” *INFORMS Journal on Computing*, 19(3), 328–340.

Varma, A. H., Ricles, J. M., Sause, R., and Lu, L.-W. (2002). “Seismic behavior and modeling of high-strength composite concrete-filled steel tube (CFT) beam–columns.” *Journal of Constructional Steel Research*, 58, 725–758.

Virdi, K. S., and Dowling, P. J. (1973). “The Ultimate Strength of Composite Columns in Biaxial Bending.” *Proceedings of the Institution of Civil Engineers*, 55(1), 251–272.

Virdi, K. S., Pilkington, J., Dowling, P., and Croft, D. (1973). "Discussion. The ultimate strength of composite columns in biaxial bending." *Proceedings of the institution of civil engineers*, 55, 739–741.

CHAPTER 2

BIAXIAL BEHAVIOR AND DESIGN OF STEEL-CONCRETE COMPOSITE COLUMNS

Abstract

Steel-concrete composite columns are strong and efficient structural members. However, their strength is not consistently recognized within design standards. In particular, current provisions regarding the strength of composite columns under combined axial compression and biaxial bending are overly simplistic and conservative. This chapter presents a study of the biaxial behavior of composite columns and methods of evaluating their strength. Analyses of composite cross sections confirm the conservative nature of current design provisions and form the basis for modified strength equations that better capture the shape of the three-dimensional interaction surface. Analyses of composite columns confirm that the proposed design equations are suitable for use within the direct analysis method for evaluating members with length effects. The proposed design equations are further validated against published experimental results. This chapter provides key insights on the behavior of composite columns subjected to axial compression and biaxial bending and offers an improved yet practical method of evaluating strength under these conditions that will enable more efficient designs.

Keywords: Steel-Concrete composite columns, Strength Interaction, Biaxial Bending, Slenderness, Beam columns

Introduction

The AISC *Specification for Structural Steel Buildings* (AISC 2016) is the primary standard governing structural design of steel-concrete composite columns for building structures in the United States. There has been significant development of the steel-concrete composite column provisions in this standard in recent editions. However, there remain several aspects of design, such as the strength of members subjected to combined axial compression and biaxial bending, where additional research and development would be beneficial.

No specific provisions are given within the AISC *Specification* (2016) for biaxial bending of composite columns. However, a method of determining the available strength in these conditions is provided in the associated commentary. Design equations for this method imply a biaxial moment (i.e., M_x-M_y) interaction diagram that is constructed with straight lines between the flexural strengths about the two principal axes, as shown in Figure 2-1. This is a simple approach, but one that is overly conservative. This is particularly true for circular concrete-filled steel tube (CCFT) members where it is expected that the M_x-M_y interaction diagram is axisymmetric. It is also true for rectangular concrete-filled steel tube (RCFT) and steel reinforced concrete (SRC) members where physical experiments (Bridge 1976; Hardika and Gardner 2004; Morino et al. 1984b; Perea et al. 2014; Shakir-Khalil and Mouli 1990; Shakir-Khalil and Zeghiche 1989; Virdi and Dowling 1973) and numerical analyses (Denavit and Hajjar 2014; Liang et al. 2012; Patel et al. 2015) show that composite columns exhibit a more convex interaction strength.

This chapter presents an investigation of the biaxial behavior of steel-concrete composite members with a focus on strength. Current methods for determining interaction strength are reviewed. Then, a broad parametric study on composite cross sections is performed to better understand the shape of the three-dimensional interaction surface and the factors that influence it. An improved strength interaction equation is proposed with a governing shape parameter calibrated to the results of the parametric study. A second parametric study on composite columns is performed to verify the use of the proposed design equation within the direct analysis method considering length effects. Lastly, the proposed equation is further validated against previously published experimental results.

Cross Section Strength

Methods of Determining Cross Section Strength

The plastic stress distribution (PSD) method is the primary method for computing the strength of composite cross sections in the AISC *Specification* (2016). Other standards, including the Eurocode (CEN 2004) and the Chinese

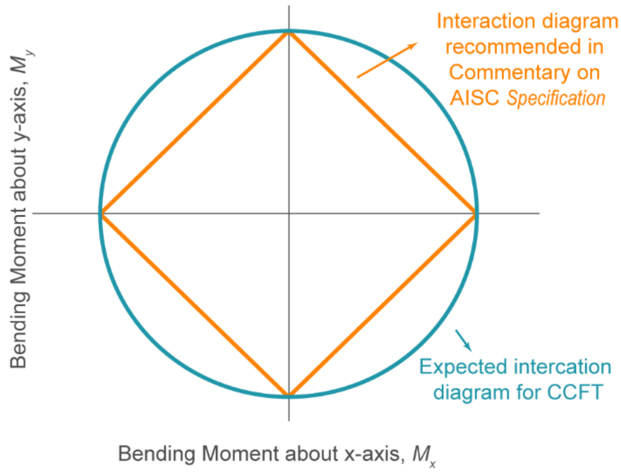

Figure 2-1. Schematic interaction diagram at a constant axial load

code for composite structures (SAC 2014), also use the PSD method for determining the strength of steel-concrete composite members. In the PSD method the entire steel section and all reinforcing bars (if present) are assumed to have reached their yield stress in either tension or compression and the concrete in compression is assumed to have attained a stress of $0.85f'_c$ (or $0.95f'_c$ for CCFT), where f'_c is the concrete compressive strength. The tension strength of concrete is neglected. Points on the interaction surface are obtained by selecting a neutral axis location and orientation then integrating the assumed stress distribution over the cross section. Numerical integration using a fiber discretization approach is used in this work to accommodate a wide range of cross sections and loading conditions. The entire interaction surface is constructed by computing many points for many locations and orientations of the neutral axis.

The PSD method can yield unconservative results, especially for SRC cross sections with high steel ratios and high steel yield strengths. A modified plastic stress distribution (MPSD) method has been recently proposed to alleviate these errors (Behnam and Denavit 2020). In this method, the interaction strength is computed per the PSD method then a factor, ψ, given by Equation 1-8 is applied to the moment strengths.

$$\psi = \varphi_1 - \varphi_2 \left(\frac{P}{P_{no}} \right) \tag{1-8}$$

where, φ_1 and φ_2 are calibration parameters defined by Equation 1-9, P is the axial compression, and P_{no} is the axial capacity of the composite cross section defined by Equation 1-10.

$$\varphi_1 = -0.15 + 0.75 \frac{A_s F_y}{P_{no}}, \varphi_2 = 1.0 - 0.15 \frac{A_s F_y}{P_{no}} \qquad (\mathrm{SRC}) \tag{1-9a}$$

$$\varphi_1 = 0.15 + 0.10 \frac{A_s F_y}{P_{no}}, \varphi_2 = 0.10 + 0.05 \frac{A_s F_y}{P_{no}} \qquad (\mathrm{RCFT}) \tag{1-9b}$$

$$P_{no} = F_y A_s + F_{ysr} A_{sr} + 0.85 f_c' A_c \quad \text{(SRC)} \tag{1-10a}$$

$$P_{no} = F_y A_s + 0.85 f_c' A_c \quad \text{(RCFT)} \tag{1-11b}$$

where, A_s, A_{sr}, and A_c are the cross-sectional areas of the steel shape, reinforcing bars, and concrete, respectively, and F_y and F_{ysr} are the yield stresses of the steel shape and reinforcing bars, respectively. Note that Equation 1-10b is applicable only to compact RCFT members without internal reinforcing.

The strain compatibility (SC) method is the main procedure for determining interaction strength in the ACI *Code* which included provisions for composite columns up until the 2014 edition (ACI 2014). This method is permitted as an alternative procedure within the AISC *Specification* (2016) for the strength of steel-concrete composite cross sections. In this method, it is assumed that the strain in the extreme concrete compressive fiber is 0.003 and the distribution of strain across the section is linear. Steel and concrete stresses are computed from defined stress-strain relationships assuming the location and orientation of the neutral axis. Just as for the PSD method, points on the interaction surface are computed by integrating the assumed stress over the cross section. For this work, an elastic-perfectly plastic relationship is used for the steel components and the rectangular stress block described in the ACI *Code* (2014) is used for the concrete. An upper limit of $0.85P_{no}$ is applied to the nominal compressive strength of the SC method as was required for composite columns in the ACI *Code* (2014).

The strength of composite cross sections can also be computed from inelastic section analysis (ISA). In this method, the cross section is discretized into a grid of fibers and each fiber is assigned a uniaxial stress-strain relationship. In this work, ISA is performed using OpenSees (McKenna et al. 2010b). The results of many analyses are used to construct each interaction diagram. Each analysis subjects the cross section to non-proportional loading to failure, specifically, an axial compressive load is applied to the section and held constant, then bending moments are applied based on a selected angle of loading in the M_x-M_y plane until a peak is reached. The peak applied loads from each analysis represent one point on the interaction surface.

The uniaxial stress-strain relationships and fiber discretizations used in this work were developed and validated in previous work (Denavit and Hajjar 2014) and have been used in similar studies (Behnam and Denavit 2020). Key details are repeated here. The maximum size of each fiber in the *x* and *y* directions is 1/30th of the outside dimension of the gross section along the *x*- and *y*-axes, respectively. For the SRC cross sections, the concrete was divided into three regions: the highly confined concrete between the flanges of the steel shape, the moderately confined concrete within the ties, and the cover concrete. The Popovics concrete stress-strain relationship was used for each, although with different levels of confinement based on the properties and geometry of the steel components. For the RCFT cross sections, a single region was used for the concrete with no consideration of confinement. Wide-flange steel shapes were assigned an elastic-perfectly plastic stress-strain relationship and residual stresses were included following the Lehigh residual stress pattern. Reinforcing steel was assigned an elastic-perfectly plastic stress-strain relationship. Steel tubes were assigned a multi-linear stress-strain relationship (Abdel-Rahman and Sivakumaran 1997).

Current Interaction Equation

The PSD, SC, and ISA methods are general methods of computing the interaction strength of composite cross sections. However, none of these methods account for member length effects. The methods of design presented in the AISC *Specification* (2016), including the direct analysis method, require available strengths that consider member stability. Current guidance suggests that a simple transformation between cross section and beam-column interaction diagrams be made by reducing the axial strength of each point by the ratio P_n/P_{no}, where P_n is the axial compressive strength of the composite member and P_{no} is given by Equation 1-1. However, this reduction leads to illogical results near the balance point where points on the beam-column interaction surface lay outside the cross section interaction surface. This is resolved with a further simplification of the interaction surface based on a few anchor points. The interaction equation recommended in the commentary of the AISC *Specification* (2016) is given by Equation 1-12 for the case of load and resistance factor design (LRFD) and without resistance factors.

for $P_u < P_{C'}$

$$\frac{M_{ux}}{M_{Cx}} + \frac{M_{uy}}{M_{Cy}} \leq 1 \tag{1-12a}$$

for $P_u \geq P_{C'}$

$$\frac{P_u - P_{C'}}{P_n - P_{C'}} + \frac{M_{ux}}{M_{Cx}} + \frac{M_{uy}}{M_{Cy}} \leq 1 \tag{1-12b}$$

where, $P_{C'}$, M_{Cx}, M_{Cy} are determined using the PSD method as the nominal axial compressive strength, nominal flexural strength about the *x*-axis, and nominal flexural strength about the *y*-axis at Point C on the interaction diagram (Point C corresponds to a plastic neutral axis location that results in the same flexural strength as pure bending but with concurrent axial compression; the axial compression at Point C is reduced by P_n/P_{no} to obtain $P_{C'}$); and P_u, M_{ux} and M_{uy} are the required axial compression strength, required flexural strength about the *x*-axis, and required flexural strength about the *y*-axis, respectively, all computed from LRFD load combinations.

Figure 2-2 illustrates two-dimensional slices of the interaction surface for an example RCFT cross section at three different axial loads as obtained from the PSD, ISA, and SC methods as well as the current design equation recommended in the commentary on the AISC *Specification* (Equation 1-12). The example RCFT cross section consists of a rectangular tube with outside height, H = 300 mm, outside width, B = 200 mm, thickness, t = 6.3 mm (this corresponds to a ratio of steel area to gross area, ρ_s = 0.1), steel yield strength, F_y = 345 MPa, and concrete strength, f'_c = 20 MPa. This cross section has no internal reinforcing.

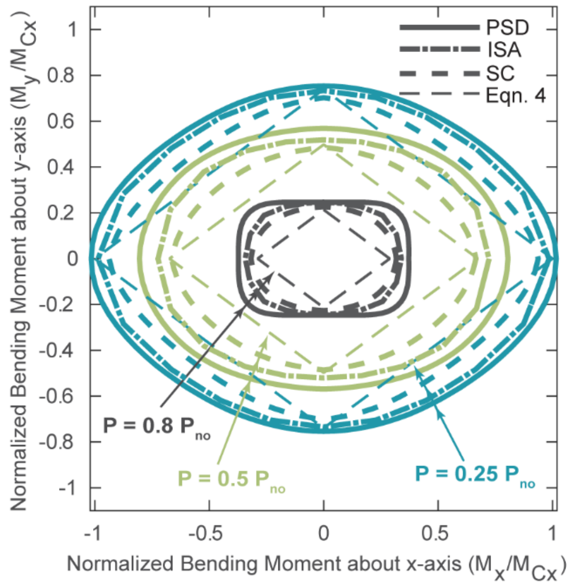

Figure 2-2. Two-dimensional interaction diagrams for an example RCFT cross section

This figure shows the conservative nature of the diamond shaped interaction diagrams resulting from the current design equation.

Generalized Interaction Equation

Equation 1-13 describes a generalized interaction surface in which the parameter α controls the shape, ranging from diamond (α = 1), to elliptical (α = 2), and further to rectangular (α = ∞), as shown in Figure 2-3.

$$\left(\frac{M_{ux}}{M_{nx}\left(P_u\right)}\right)^{\alpha}+\left(\frac{M_{uy}}{M_{ny}\left(P_u\right)}\right)^{\alpha}\leq 1 \qquad (1\text{-}13)$$

where, $M_{nx}(P_u)$ and $M_{ny}(P_u)$ are the nominal moment strengths about the *x*-axis and *y*-axis, respectively, at the required axial compression strength, P_u.
This interaction equation is one of several that are commonly used for the assessment of reinforced concrete columns (Furlong et al. 2004). While biaxial strengths computed from the PSD, SC, and ISA methods will not conform precisely to Equation 1-13, identifying the best fit α parameter is an effective way of quantifying the shape of the curve and can lead to important insights. The best fit shape parameter is computed through the solution of an optimization problem for a given cross section and axial load. The objective function for this optimization, Equation 1-14, is defined as the mean squared error (*MSE*) between the computed strength (i.e., from the PSD, SC, or ISA method) and the strength from the generalized interaction equation.

$$MSE=\frac{1}{N}\sum_{\theta}\left(M_{n\theta 1}-M_{n\theta 2}\right)^{2} \qquad (1\text{-}14)$$

where, $M_{n\theta 1}$ is the nominal flexural strength computed from the PSD, SC, or ISA method about an axis defined by angle θ in the M_x-M_y plane, $M_{n\theta 2}$ is the nominal flexural strength about the same axis but obtained using Equation 1-13, and *N* is the number of angles in the M_x-M_y plane that are sampled (9 in this work).

The goal of this optimization is to quantify the shape of the interaction equation. Thus, when evaluating $M_{n\theta 2}$, the values of the strengths about the *x*- and *y*-axes (i.e., M_{nx} and M_{ny}) were taken as those obtained from the methods

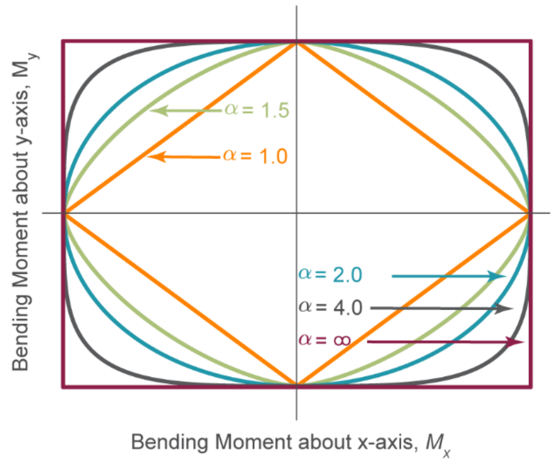

Figure 2-3. Variation of generalized interaction equation with shape parameter α

under investigation. With this assumption, $M_{n\theta 2}$ can be computed using Equation 1-15.

$$M_{n\theta 2}=\left(\left(\frac{\cos(\theta)}{M_{nx1}}\right)^{\alpha}+\left(\frac{\sin(\theta)}{M_{ny1}}\right)^{\alpha}\right)^{-1/\alpha} \qquad (1\text{-}15)$$

where, M_{nx1} and M_{ny1} are the nominal moment strengths about the *x*-axis and *y*-axis, respectively, computed from the PSD, SC, or ISA method and at the given axial load.

The best fit α was obtained such that *MSE* (Equation 1-14) reached its minimum value and was found using a built-in optimization function in MATLAB based on golden section search and parabolic interpolation (Brent 2013; Forsythe et al. 1977). Figure 2-4 shows the best fit α versus normalized axial load for each of the three methods of obtaining the interaction strength and for the example RCFT cross section described previously. For each of the methods, α initially decreases with increasing axial load, reaching a minimum for an axial load of about $0.2P_{no}$ before increasing with increasing axial load. For this cross section, the lowest value of α was determined to be 1.69, 1.63, and 1.42, for the PSD, ISA, and SC methods, respectively. Each of these values is significantly greater than the α = 1.0 implied by the current design equation (Equation 1-12).

Parametric Study

A parametric study was performed to capture the wide range of behavior expected from composite cross sections with different steel ratios, material strengths, and other parameters. Suites of RCFT and SRC cross sections were defined and three-dimensional interaction surfaces were computed for each using the PSD, SC, and ISA methods. Then, the best fit shape parameter α was computed for each interaction surface and for axial compressive loads ranging from zero to $0.8P_{no}$.

A total of 3,408 RCFT cross sections were investigated in this study. As

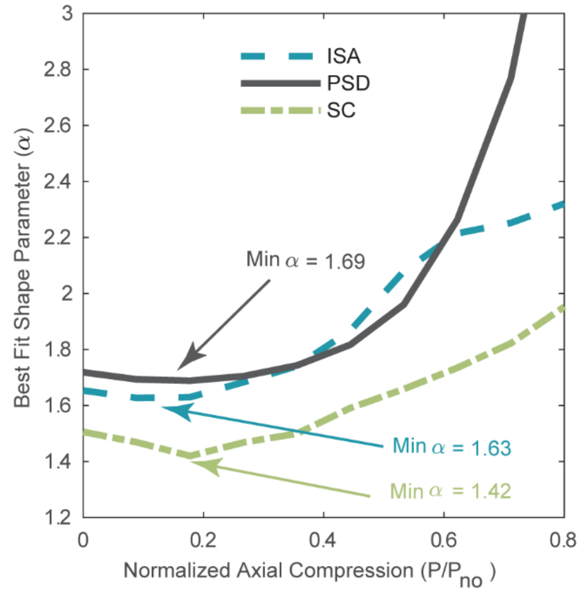

Figure 2-4. Variation of best fit α with normalized axial compression for an example RCFT cross section

described in Table 2-1, the selected cross sections vary in aspect ratio (H/B), steel ratio (ρ_s), steel yield stress (F_y), and concrete compressive strength (f'_c). The width and thickness of the steel tube were computed based on the aspect ratio, steel ratio, and H = 305 mm. The height, H, was constant for all cross sections. The product of the number of variations for each parameter in Table 2-1 is 4,032; however, since local buckling of the steel tube is not considered in this work, only sections that are classified as compact by the AISC *Specification* (2016) were considered. Specifically, the 624 cross sections that did not satisfy the inequality of Equation 1-16 were omitted from the study.

$$\frac{H-3t}{t} \leq 2.26\sqrt{\frac{E_s}{F_y}} \tag{1-16}$$

where, E_s is the modulus of elasticity of steel equal to 200,000 MPa.

A total of 14,688 SRC cross sections were investigated in this study. As described in Table 2-2, the selected cross sections vary in aspect ratio (H/B), steel shape, steel yield stress (F_y), concrete compressive strength (f'_c), reinforcing configuration, and reinforcing yield stress (F_{yr}). The gross area was taken as A_g = 819,025 mm^2 for all cross sections. The longitudinal reinforcing bars were assumed to be arranged symmetrically in the corners with a clear spacing equal to the greater of 38 mm or 1.5 times the diameter of the bar. For square cross sections, the number of bars along each face was equal, while for sections with larger aspect ratios, the number of bars along the longer face was greater as described in Table 2-3 where the reinforcing configuration identifies the number of bars along the x- and y-axes of the cross section. The clear cover between the ties and the outside surface of the concrete was taken as 38 mm. The size of the tie bars was based on the size of the longitudinal bars, #3 and #4 tie bars were used with #10 and #11 longitudinal bars, respectively. The tie spacing was assumed to be 305 mm. The product of the number of variations for each parameter in Table 2-2 is 17,280. However, 2,592 cross sections were omitted from the study because the spacing requirements could not be met as described in the footnotes to Table 2-3.

Table 2-1. Selected parameters for the RCFT cross sections

Parameter	Values
Cross section aspect ratio[1], H/B	1.0, 1.25, 1.5, 1.75, 2.0, 2.5, and 3.0
Steel ratio, ρ_s	0.08, 0.10– 0.40 (increments of 0.05)
Steel yield stress, F_y	240–520 MPa (increments of 35 MPa)
Concrete compressive strength, f'_c	20–69 MPa (increments of 7 MPa)

Table 2-2. Selected parameters for the SRC cross sections

Parameter	Values
Cross section aspect ratio, H/B	1.0, 1.25, 1.5, 1.75, and 2.0
Steel shape (ASTM A6 2019)	W14×873, W14×665, W14×455, W14×211, W14×176, W14×132, W14×90, and W10×49 (ρ_s = 0.198, 0.151, 0.103, 0.048, 0.040, 0.030, 0.020, and 0.011)
Steel yield stress, F_y	240–520 MPa (increments of 35 MPa)
Concrete compressive strength, f'_c	20–69 MPa (increments of 7 MPa)
Reinforcing configuration (ASTM A615 2020)	(12) #10, (20) #11, and (28) #11 (A_{sr}/A_g = 0.012, 0.024, and 0.034)
Reinforcing yield stress, F_{ysr}	280 MPa and 420 MPa

Table 2-3. Reinforcement configurations for SRC cross sections

Cross section aspect ratio	Reinforcing Configuration		
	(12) #10	(20) #11	(28) #11
1.0	4x-4y	6x-6y	8x-8y
1.25	4x-4y	6x-6y	6x-10y
1.5	4x-4y	6x-6y [1]	6x-10y [1]
1.75	4x-4y	4x-8y [2]	6x-10y [2]
2.0	4x-4y [3]	4x-8y [3]	6x-10y [4]

[1] Not used with ρ_s = 0.198
[2] Not used with $\rho_s \geq$ 0.103
[3] Not used with $\rho_s \geq$ 0.151
[4] Not used with $\rho_s \geq$ 0.04

The range of best fit shape parameter α for all cross sections studied is shown in Figure 2-5. In this figure, the minimum value of the best fit α from each method and each cross section type is plotted versus normalized axial compression load. The 10th percentile, 50th percentile (i.e., median), 90th percentile, and maximum values of the best fit α are also plotted. Wide variations in the value of the best fit α, and correspondingly the shape of the interaction diagram, can be seen at low axial loads and at high axial loads. There is also significant variation in the shape of the interaction surfaces as obtained from the different methods. The SC method exhibits the lowest values of α and the PSD method exhibits the highest values of α. For some SRC sections, a best fit α less than unity is seen with the SC method, indicating a somewhat concave interaction diagram.

Variation of the best fit α was also noted for other parameters. For example, the variation of the minimum best fit α for RCFT sections computed using the ISA method with respect to the steel ratio is shown in Figure 2-6. This result shows that the absolute minimum of α = 1.52 occurred at a relatively low steel ratio and sections with higher steel ratios had greater minimums.

Proposed Design Equation

Given the preceding discussion, it is clear that the shape of the interaction surface currently given in the commentary on the AISC *Specification* (2016) for steel-concrete composite columns is conservative for biaxial bending. A direct construction of the three-dimensional interaction surface using the PSD or SC method would be more accurate for short columns in many cases. However, these methods cannot be used for slender columns due to a lack of justifiable methods of reducing the interaction surface for length effects. Also, equations that rely on only a few key anchor points are simple and efficient to use. The generality and ease of use of the current equation can be maintained in a less overly conservative fashion with a modification to include the shape parameter, α, as shown in Equation 1-17.

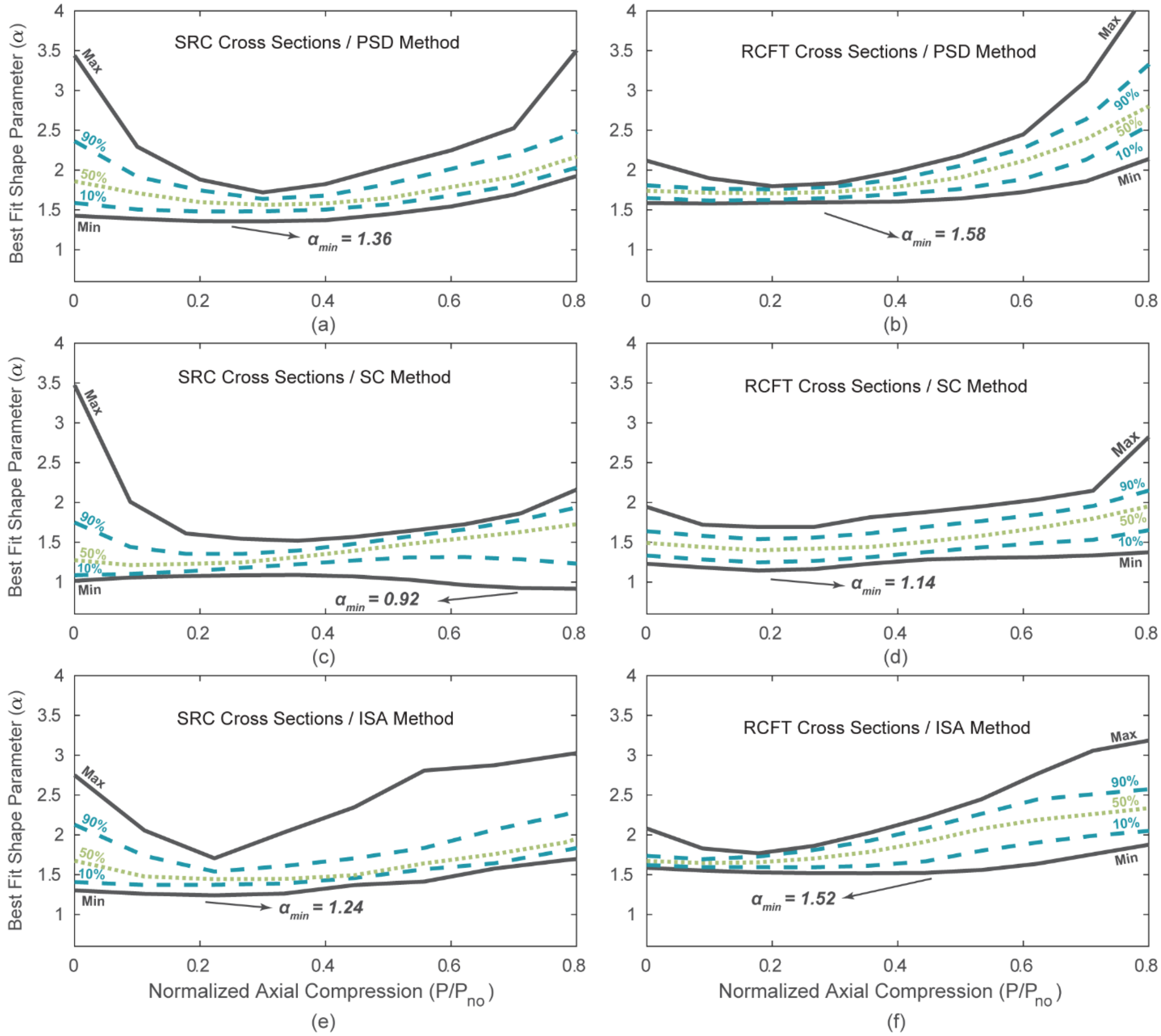

Figure 2-5. Variation of best fit α with normalized axial compression for all cross sections

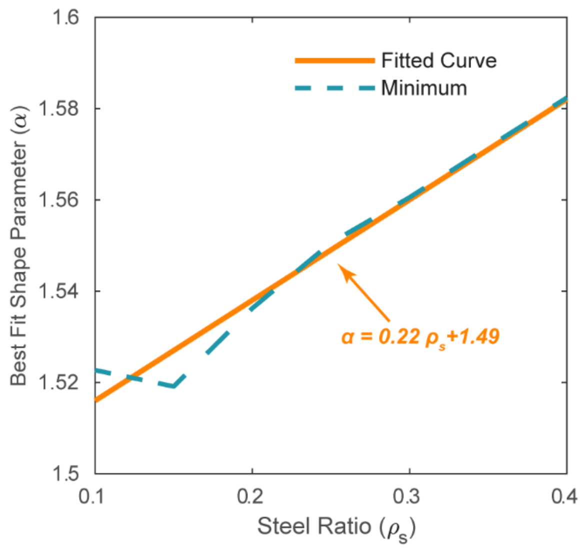

Figure 2-6. Variation of best fit α from the ISA method for RCFT cross sections with steel ratio

for $P_u < P_{C'}$

$$\left(\frac{M_{ux}}{M_{Cx}}\right)^{\alpha} + \left(\frac{M_{uy}}{M_{Cy}}\right)^{\alpha} \le 1 \tag{1-17a}$$

for $P_u \ge P_{C'}$

$$\frac{P_u - P_{C'}}{P_n - P_{C'}} + \left(\frac{M_{ux}}{M_{Cx}}\right)^{\alpha} + \left(\frac{M_{uy}}{M_{Cy}}\right)^{\alpha} \le 1 \tag{1-17b}$$

Equation 1-17 reduces to the current design equation if the shape parameter is set to unity (i.e., $\alpha = 1.0$). As seen in the preceding analyses, α varies with the level of axial loading and cross-sectional properties. However, for simplicity this value can be taken as $\alpha = 1.25$ for SRC and $\alpha = 1.5$ for RCFT based on the minimum best fit α from the ISA method (Figure 2-5). The SC method exhibits lower values of α, but this method is notably conservative for steel-concrete composite columns (Behnam and Denavit 2020). Additionally, based on the axisymmetric nature of CCFT cross sections, it is expected that the shape parameter can be taken as $\alpha = 2.0$ for CCFT.

Given that α was calibrated based on the shape of the interaction surface, the accuracy of Equation 1-17 relies on the accuracy of the anchor points P_n, $P_{C'}$, M_{Cx}, and M_{Cy}. It should be noted that $P_{C'}$, M_{Cx}, and M_{Cy} in Equation 1-17 are typically computed using the PSD method. Behnam and Denavit (2020) showed that the PSD method can be unconservative in some situations. Applying the modification factor of Equation 1-18 to M_{Cx} and M_{Cy} will reduce these potential errors and improve the accuracy of Equation 1-17 overall. A quantification of the accuracy of Equation 1-17 through comparisons to analyses including length effects and physical experiments is presented in the following sections.

Beam-Column Strength

A second parametric study, including length effects, is performed to verify that the proposed design equation is safe and accurate for use in design with the direct analysis method as defined within the AISC *Specification* (2016). Following the general procedure used in other evaluations of stability design provisions

(Kanchanalai 1977; MacGregor and Hage 1977; Surovek-Maleck and White 2004; Denavit et al. 2016b), results of second-order inelastic analyses are compared to results from the design procedure, which in the case of the direct analysis method is based on second-order elastic analysis. The comparisons are made for a large number of simple frames covering a wide range of parameters.

Parametric Suite

Many parameters influence the strength of composite columns. They can be broadly classified as those associated with the cross section, including type, steel ratio, and material strengths; and those associated with the frame, including slenderness, boundary conditions, and leaning column load. A parametric study is essential to cover this wide range of parameters. The parametric suite of frames used in this work is based on the suite used by Denavit et al. (2016b), which itself was based on parametric suites from previous studies (Kanchanalai 1977; Surovek-Maleck and White 2004). Each of these previous studies investigated two-dimensional behavior, thus modifications were necessary to investigate three-dimensional behavior including biaxial bending.

Three types of frames, as shown in Figure 2-7, are included in the suite. For the first type of frame, Type A, the composite column is braced (sidesway inhibited) in both directions. For Type B frames, the composite column is unbraced (sidesway uninhibited) in both directions. For Type C frames, the composite column is unbraced in the *yz* plane and braced in the *xz* plane. For each type of frame, vertical applied loads are defined by P and lateral applied loads are defined by X. As shown in Figure 2-7, X is factored by defined parameters to obtain applied lateral loads and bending moments as appropriate for the frame type.

Type A frames are defined by a slenderness ratio, λ, and end moment ratios in each of the coordinate axes, $M_{bot,x}/M_{top,x}$ and $M_{bot,y}/M_{top,y}$. When

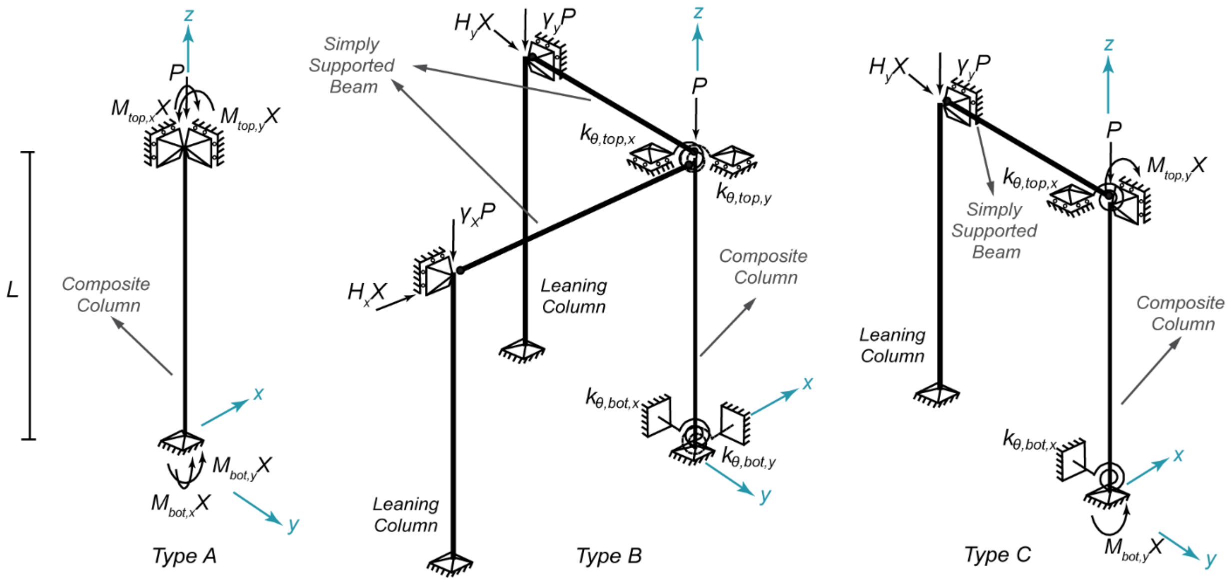

Figure 2-7. Schematic of the three-dimensional benchmark frames

negative, the end moment ratios produce single curvature bending. The slenderness ratio, λ, is defined by Equation 1-19 as the length divided by the geometric mean of the lateral dimensions of the cross section.

$$\lambda = \frac{L}{\sqrt{HB}} \tag{1-19}$$

where, *L* is the length of the column.

Type B frames are defined by a slenderness ratio (Equation 1-19), leaning column load ratio in each of the two coordinate planes (γ_x and γ_y), and end restraint parameters (G_{top} and G_{bot}). The two leaning columns included in the model are pinned at the bottom and constrained at the top in one direction to the composite column. The two pairs of rotational springs at the top and bottom of the composite column provide stability to the member and are representative of the beams that frame into the column. The stiffness of the rotational springs is defined by the end restraint parameters in accordance with Equation 1-20.

$$\begin{aligned} k_{\theta,top,x} &= \frac{6EI_{eff,x}}{G_{top}L}, \quad k_{\theta,bot,x} = \frac{6EI_{eff,x}}{G_{bot}L} \\ k_{\theta,top,y} &= \frac{6EI_{eff,y}}{G_{top}L}, \quad k_{\theta,bot,y} = \frac{6EI_{eff,y}}{G_{bot}L} \end{aligned} \tag{1-20}$$

where, $EI_{eff,x}$ and $EI_{eff,y}$ are the effective elastic rigidities about the *x*- and *y*-axes, respectively, as defined in the AISC *Specification* (2016) and in Equation 1-21.

$$EI_{eff} = E_s I_s + E_s I_{sr} + C_1 E_c I_c \qquad \text{(SRC)} \tag{1-21a}$$

$$EI_{eff} = E_s I_s + C_3 E_c I_c \qquad \text{(RCFT)} \tag{1-21b}$$

where, E_c is the modulus of elasticity of concrete defined by Equation 1-22, I_s, I_{sr}, and I_c are the moment of inertia of the steel shape, reinforcing bars, and concrete, respectively, and C_1 and C_3 are coefficients defined by Equations 1-23 and 1-24, respectively.

$$E_C(\text{MPa}) = 4733\sqrt{f_c^{'}(\text{MPa})} \tag{1-22}$$

$$C_1 = 0.25 + 3\left(\frac{A_s + A_{sr}}{A_g}\right) \le 0.7 \tag{1-23}$$

$$C_3 = 0.45 + 3\left(\frac{A_s + A_{sr}}{A_g}\right) \le 0.9 \tag{1-24}$$

Type C frames are defined by the parameters for Type A frames in the *xz* plane and the parameters for Type B frames in the *yz* plane. The selected parameters for each frame type are described in Table 2-4 and Table 2-5. In total, 168 different sets of parameters are selected among the three frame types. A variety of loading angles were analyzed for each case. Different loading angles were achieved by selecting appropriate relative values for the parameters that control the lateral load. For example, $M_{bot,x}$ and $M_{bot,y}$ for Type A frames and H_x and H_y for Type B frames. The loading angle was defined by applied loading noting that the relative values of the internal moments along the length of the member may differ from those that are applied.

Each of the 168 selected sets of frame parameters is used with each selected cross section to form the parametric suite. Noting this and the fact that the column analyses are more time consuming than the cross section analyses, a smaller set of cross sections was selected for investigation than was selected for the parametric study on cross sections presented previously. The cross sections selected for this parametric study are based on those from a previous study (Denavit et al. 2016b).

The selected RCFT cross sections vary in the steel tube and concrete strength. Seven steel tubes were selected for this work: HSS6×6×1/2, HSS9×9×1/2, HSS8×8×1/4, HSS10×5×3/8, HSS10×5×3/16 (ASTM A500 2020). These steel tubes result in steel ratios of ρ_s = 0.28, 0.19, 0.11, 0.19, and 0.10, respectively. Note that the design thickness, equal to 0.93 times the nominal thickness, was utilized for all analyses and calculations. Each cross section was assumed to have a yield stress of F_y = 317 MPa. Two concrete strengths of f'_c = 27.6 and 68.9 MPa were investigated to include the effect of normal and high strength concrete.

The selected SRC cross sections vary in steel shape, reinforcing

Table 2-4. Selected frame parameters for the beam-column parametric study

Frame	Slenderness	End Condition (yz plane)	End Condition (xz Plane)	Leaning Column Load Ratio	Number of Frames
A	3 values $\lambda = \{12,24,36\}$	2 values $M_{bot,x}/M_{top,x} = \{0.5, -1.0\}$	2 values $M_{bot,y}/M_{top,y} = \{0.5, -1.0\}$	N/A	12
B	3 values $\lambda = \{6,12,24\}$	4 value pairs A, B, C, D (Table 2-5)	4 value pairs A, B, C, D (Table 2-5)	1 value $\gamma_x = \gamma_y = 0$	48
B	2 values $\lambda = \{6,12\}$	4 value pairs A, B, C, D (Table 2-5)	4 value pairs A, B, C, D (Table 2-5)	2 values $\gamma_x = \gamma_y = \{1,3\}$	64
B	1 values $\lambda = \{24\}$	2 value pairs A, B (Table 2-5)	2 value pairs A, B (Table 2-5)	2 values $\gamma_x = \gamma_y = \{1,3\}$	8
C	3 values $\lambda = \{6,12,24\}$	4 value pairs A, B, C, D (Table 2-5)	2 values $M_{bot,y}/M_{top,y} = \{0.5, -1.0\}$	1 value $\gamma_x = 0$	24
C	3 values $\lambda = \{6,12,24\}$	1 value pair A (Table 2-5)	2 values $M_{bot,y}/M_{top,y} = \{0.5, -1.0\}$	2 values $\gamma_x = \{1,3\}$	12

Table 2-5. End Restraint Value Pairs

Pair	G_{top}	G_{bot}
A	0	0
B	1 or 3[a]	1 or 3[a]
C	0	∞
D	1 or 3	∞

[a]3 when $\gamma = 0$; 1 otherwise

configuration, and concrete strength. The outside dimensions of each was selected to be 711 mm × 711 mm. Four steel shapes were selected for this study: W14×311, W14×233, W12×120, and W8×31 (ASTM A6 2019). These steel shapes result in steel ratios of ρ_s = 0.127, 0.087, 0.045, and 0.012, respectively. The steel shapes were assumed to have a yield stress of F_y = 345 MPa. Three reinforcing configurations were selected: (20) #11, (12) #10, and (4) #8 (ASTM A615 2020) resulting in reinforcing steel ratios of A_{sr}/A_g = 0.040, 0.019, and 0.004, respectively. The reinforcing bars were assumed to have a yield stress of F_{yr} = 414 MPa. The cover and reinforcement spacing were the same as described previously for the parametric study on cross sections. Two concrete strengths of f'_c = 27.6 and 68.9 MPa were investigated.

A total of 14 RCFT cross sections and 24 SRC cross sections were investigated in this study. Together with the 168 sets of frame parameters, a total of 2,352 RCFT cases and 4,032 SRC cases were included in the parametric suite.

Second-Order Inelastic Analysis

The composite columns were modeled with a distributed plasticity mixed beam finite-element formulation implemented in the OpenSees framework (McKenna et al. 2010b). Material and geometric nonlinearities were captured using fiber sections along the member length and a total Lagrangian formulation in the corotational frame, respectively. Large displacement and rotation behavior along the length of the column are captured accurately using multiple elements. The composite columns were discretized using six elements along the member and three integration points were used per element. Slip between steel and concrete elements and local buckling of the steel tube and other steel components are neglected. The constitutive relationships and fiber discretization of the cross sections used in the second-order inelastic analyses are the same as those described previously for the inelastic section analysis (ISA) method.

An out-of-plumbness of L/500 was included in the sidesway uninhibited frames and a half-sine shaped out-of-straightness with maximum magnitude of L/1000 was included in all composite columns. These initial geometric imperfections were modeled explicitly by definition of nodal coordinates. The direction of the imperfections was that which caused the most destabilizing effect. This direction was found by performing analyses with initial imperfections in the x direction, y direction, and the direction of lateral loading then using the results of the analysis that exhibited the lowest strength.

A stiff truss element was used to model the leaning column in the sidesway uninhibited frames, and a numerical constraint was used in lieu of the simply supported beam to connect the top of the leaning column to the top of the composite column. The limit point for the inelastic analyses was defined as when the lowest eigenvalue of the system becomes negative, or the maximum absolute strain in any section of any element along the composite column reaches 0.05, whichever occurs first.

Second-Order Elastic Analysis

The mixed beam finite element formulation was also used to perform second-order elastic analysis. For the elastic analyses, the fiber sections were replaced with defined axial and flexural rigidities. Stiffnesses used for the elastic analyses were in accordance with the AISC *Specification* (2016) for the direct analysis method. Specifically, the flexural rigidity was taken as $0.64EI_{eff}$, where EI_{eff} is given by Equation 1-21, and the axial rigidity was computed using Equation 1-25, noting that A_{sr} = 0 for all RCFT cross sections investigated in this work.

$$EA = 0.8\left(E_s A_s + E_s A_{sr} + E_c A_c\right) \tag{1-25}$$

To better mimic how the direct analysis method is typically implemented, the frames were modeled without initial geometric imperfection. Rather, a notional load of 0.002 times the total axial load (i.e., the axial load on the composite column plus the leaning columns) was added in sidesway uninhibited cases. For Type B frames, the notional load was applied in the *x* direction, *y* direction, and direction of lateral loading to find the most destabilizing effect. For Type C frames, the notional load was applied only in the *y* direction.

Method of Evaluating Elastic Design Procedures

The accuracy of the design procedure is evaluated against results of second-order inelastic analyses. However, simply comparing the maximum internal forces at the peak strength from the second-order inelastic analyses to Equations 1-12 or 1-17 would be inappropriate. The internal forces from the second-order inelastic analyses depend on deformations. Given that in the design method the members are modeled differently (e.g., as elastic and with a flexural stiffness of $0.64EI_{eff}$), the internal forces would be predicted differently. A fair comparison can be made using internal forces by adjusting the results of the second-order inelastic analyses to account for the difference in deformations (Kanchanalai 1977). Another fair comparison can be made at the applied load level (Surovek-Maleck and White 2004; Denavit et al. 2016b), directly comparing the loads which cause failure according to the second-order inelastic analysis to the maximum permitted applied loads according to the design methodology. To accomplish this comparison, four separate interaction surfaces, labeled 1 through 4, are developed.

Interaction surfaces 1 and 2 are obtained from the second-order inelastic analyses. Surface 1 corresponds to the applied loads at the limit point and surface 2 corresponds to internal forces at the limit point. Many analyses are performed for each frame to construct these surfaces. An initial analysis with only axial load applied is performed. Then, many analyses are performed with applied lateral and axial loads for a range of axial loads between zero and the limit point from the axial only analysis and a range of lateral loading angles. For each of these analyses, the axial compression is applied under load control then held constant. Following that, the lateral load is applied in displacement control until the limit point is reached. The applied loads at the limit point are recorded as surface 1. For sidesway inhibited frames, the applied lateral load is converted to a moment by a simplified first order analysis, for example by multiplying by $L/2$ when rotational restraint at the top and bottom of the column are equal. The axial compression and maximum bending moments along the length of the column are recorded as surface 2.

Interaction surfaces 3 and 4 are obtained from the design methodology. Surface 3 is defined by the design strength equations (Equation 1-12 or 1-17). Surface 4 corresponds to the maximum applied forces permitted by the design methodology. Second-order elastic analyses are performed with a range of axial loads and a range of loading angles. After each analysis, internal forces recorded as the loading was ramped up are fed into the design equation to identify when the design limit was reached. The applied loads at the design limit are recorded as surface 4. As with surface 1, for sidesway inhibited frames, the applied lateral load is converted to a moment by a simplified first order analysis.

The four interaction surfaces for three example frames are shown in Figure 2-8. The same RCFT cross section is used for all three frames (HSS8×8×1/4 steel shape with f'_c = 27.6 MPa from the parametric suite). The frames are all Type A (sidesway inhibited in both directions) with $M_{top,z}/M_{bot,z} = M_{top,y}/M_{bot,y} = -1$ (resulting in single curvature moment). The frames differ only in the length of the column, with L/H = 12, 24, and 36.

The design procedure is evaluated by comparing interaction surfaces 1 and 4. These surfaces are compared in Figure 2-9 for the L/H = 24 case from Figure 2-8. Points inside surface 1 represent combinations of applied axial and lateral loads that the second-order inelastic analysis shows can be supported by the frame. Similarly, points inside surface 4 represent combinations of applied axial and lateral loads that the design methodology permits to be applied to the frame.

It is conservative when surface 4 is inside of surface 1, and unconservative otherwise. The difference between the two surfaces, the error in

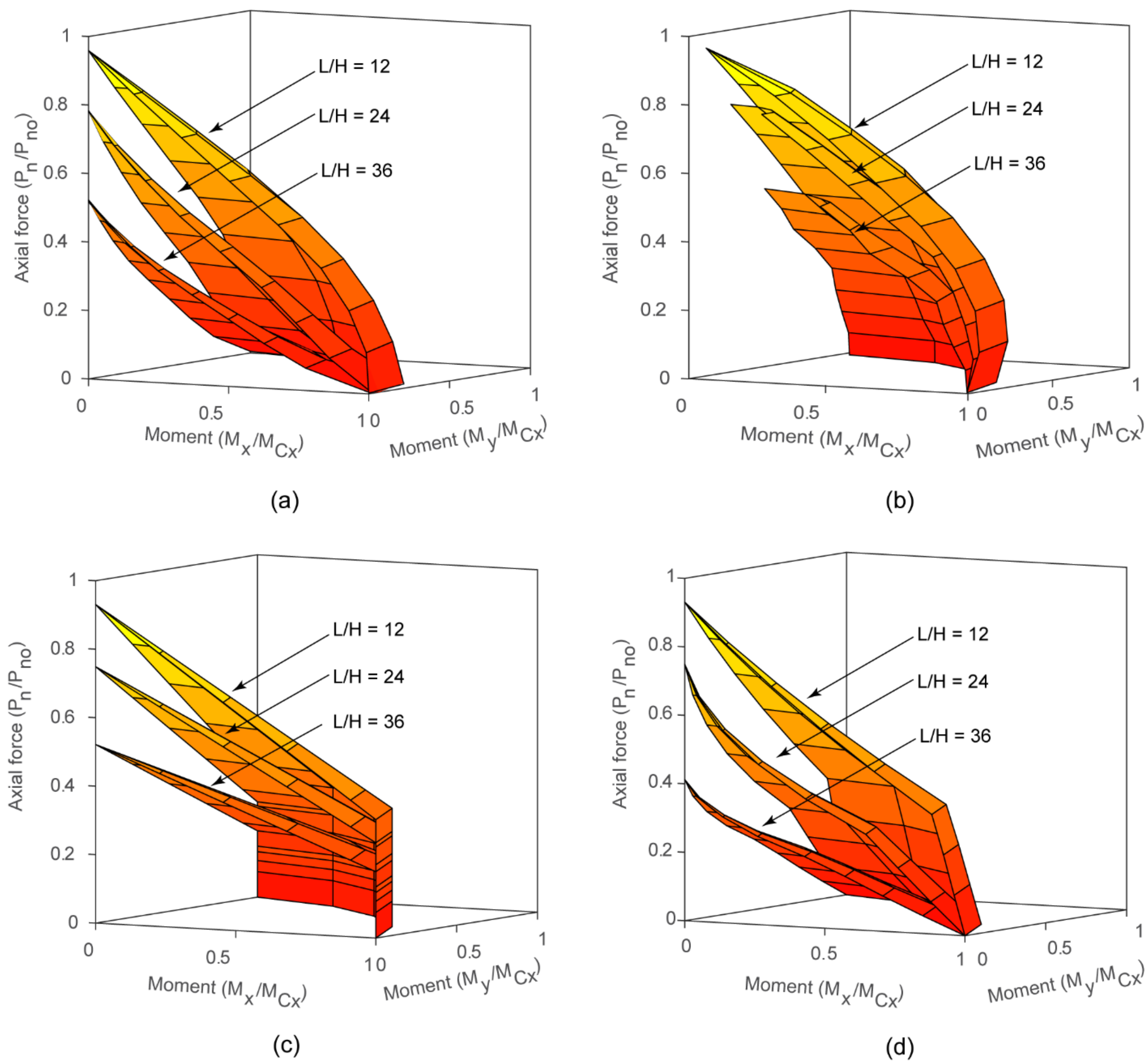

Figure 2-8. Interaction surfaces for three example RCFT frames, a) Maximum applied loads determined by second-order inelastic analysis (surface 1), b) Maximum internal forces determined by second-order inelastic analysis (surface 2), c) Design equation for the beam-column strength calculated by Equation 1-17 with α = 1.5 (surface 3), d) Maximum applied loads permitted by the proposed methodology (surface 4)

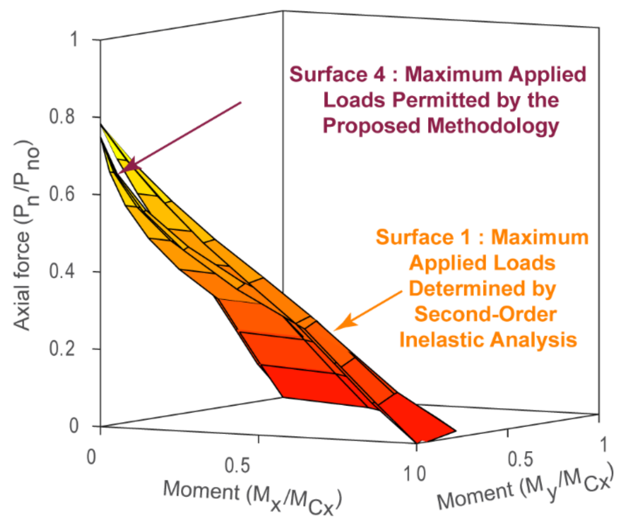

Figure 2-9. Comparison between interaction surfaces from inelastic analysis and the design methodology

the design methodology, is quantified with a radial measurement defined by Equation 1-26.

$$\varepsilon = \frac{r_1 - r_4}{r_1} \tag{1-26}$$

where r_1 is the distance along a line from the origin to interaction surface 1 and r_4 is the distance along the same line from the origin to interaction surface 4. Negative values of ε are unconservative.

Results

The four interaction surfaces were computed for each of the frames in the parametric suite. Different versions of interaction surface 4 were computed to investigate different options in the design methodology. Error in the design methodology was computed for each frame, each angle investigated in the M_x-M_y plane, and in 1-degree increments in the M_θ-P plane where P is normalized by the pure axial strength from the inelastic analysis and M_θ is normalized by the pure bending moment strength about the θ-axis from the inelastic analysis. The computed errors were then separated into bins based on steel ratio, slenderness ratio, and loading region (i.e., high moment region, intermediate region, and high axial region as shown in

Figure 2-10 2-10. The slenderness ratio used for this display of results, λ_{ana}, was taken as the value of slenderness λ_{oe} that when used in the column curve from the AISC *Specification* (2016) (Equation 1-27) results in a nominal axial compressive strength, P_n, equal to the maximum applied load from the axial-only second-order inelastic analysis.

$$P_n = \begin{cases} 0.658^{\lambda_{oe}^2} P_{no} & \text{when} \quad \lambda_{oe}^2 \le 2.25 \\ 0.877 P_{no} / \lambda_{oe}^2 & \text{when} \quad \lambda_{oe}^2 > 2.25 \end{cases} \tag{1-27}$$

This slenderness ratio, λ_{ana}, characterizes the slenderness of the frame as a whole better than λ (Equation 1-19), especially for frames with leaning column

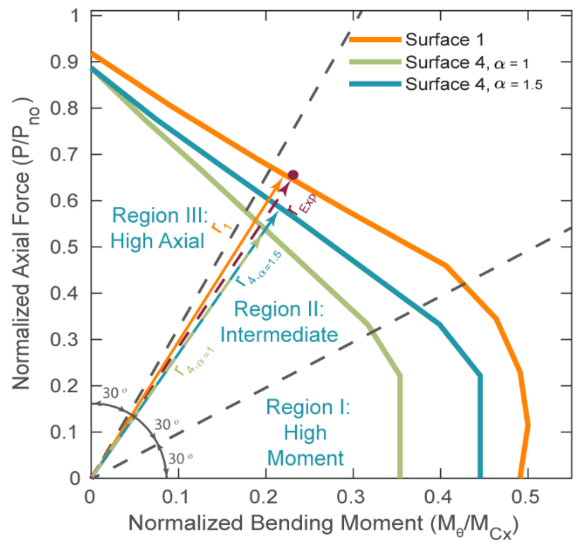

Figure 2-10. Computation of error for design methods

Table 2-6. Summary of computed error for RCFT frames using proposed interaction equation with anchor points computed using the PSD method

		$\lambda_{ana} \leq 0.5$			$0.5 \leq \lambda_{ana} \leq 1.0$			$1.0 \leq \lambda_{ana}$		
Region		I	II	III	I	II	III	I	II	III
ρ_s = 0.11	Max	25.4%	23.2%	29.9%	25.1%	25.2%	30.5%	26.3%	33.0%	39.7%
	Avg.	10.1%	5.1%	6.2%	10.3%	9.1%	9.1%	8.3%	13.7%	19.4%
	Min	-4.7%	-3.3%	-1.5%	-3.8%	-3.3%	-3.0%	-5.6%	-3.3%	-3.0%
ρ_s = 0.19	Max	17.8%	17.2%	25.8%	19.2%	22.6%	28.0%	26.0%	37.8%	36.4%
	Avg.	7.1%	7.1%	6.2%	7.3%	8.0%	7.8%	7.2%	12.2%	18.1%
	Min	-3.3%	-2.9%	-0.9%	-4.8%	-4.6%	-3.5%	-3.3%	-2.6%	3.0%
ρ_s = 0.28	Max	21.1%	21.5%	24.1%	24.5%	25.5%	23.3%	21.3%	26.2%	35.9%
	Avg.	9.7%	11.2%	7.6%	9.2%	10.7%	9.1%	9.2%	13.0%	18.6%
	Min	-2.7%	-0.7%	-0.8%	0.2%	-0.8%	-2.1%	-0.4%	-0.4%	3.2%

Table 2-7. Summary of computed error for SRC frames using proposed interaction equation with anchor points computed using the PSD method

		$\lambda_{ana} \leq 0.5$			$0.5 \leq \lambda_{ana} \leq 1.0$			$1.0 \leq \lambda_{ana}$		
Region		I	II	III	I	II	III	I	II	III
ρ_s = 0.01	Max	72.4%	70.1%	67.4%	72.9%	73.2%	74.0%	73.4%	74.2%	75.3%
	Avg.	31.2%	25.7%	21.9%	31.3%	38.5%	38.6%	24.6%	35.2%	41.8%
	Min	-6.4%	-5.4%	-2.3%	0.1%	-2.7%	7.3%	-9.9%	-8.1%	0.2%
ρ_s = 0.04	Max	42.7%	41.9%	34.4%	48.3%	49.6%	53.4%	52.6%	61.3%	64.2%
	Avg.	13.9%	13.7%	15.0%	15.7%	22.9%	25.9%	12.1%	23.2%	33.0%
	Min	-9.6%	-7.0%	-0.2%	-5.9%	-4.7%	4.5%	-9.0%	-4.0%	0.1%
ρ_s = 0.09	Max	30.6%	29.4%	28.1%	31.2%	35.0%	39.2%	31.5%	47.9%	53.2%
	Avg.	8.1%	9.4%	12.2%	7.8%	13.3%	18.1%	6.8%	15.0%	24.2%
	Min	-14.8%	-9.7%	-3.8%	-15.3%	-12.8%	-1.7%	-12.6%	-12.9%	2.6%
ρ_s = 0.12	Max	22.4%	25.0%	24.9%	22.9%	28.0%	35.6%	24.7%	40.0%	47.3%
	Avg.	4.9%	7.8%	10.7%	4.6%	9.9%	15.0%	4.3%	11.2%	20.1%
	Min	-17.9%	-8.7%	-2.7%	-17.6%	-13.6%	-5.0%	-16.8%	-16.7%	-3.0%

Table 2-8. Summary of computed error for SRC frames using proposed interaction equation with anchor points computed using the MPSD method

		$\lambda_{ana} \leq 0.5$			$0.5 \leq \lambda_{ana} \leq 1.0$			$1.0 \leq \lambda_{ana}$		
Region		I	II	III	I	II	III	I	II	III
ρ_s = 0.01	Max	72.4%	70.1%	67.4%	72.9%	73.2%	74.0%	73.4%	74.2%	75.3%
	Avg.	31.5%	25.7%	21.8%	31.7%	38.6%	38.6%	25.1%	35.3%	41.8%
	Min	-6.4%	-5.4%	-2.3%	0.1%	-2.7%	7.3%	-9.2%	-7.5%	0.4%
ρ_s = 0.04	Max	44.2%	43.1%	35.2%	49.4%	50.4%	53.6%	52.8%	61.4%	64.3%
	Avg.	18.1%	16.3%	16.1%	19.2%	25.3%	27.1%	15.1%	24.8%	33.6%
	Min	-7.5%	-6.1%	0.0%	-3.5%	-3.0%	6.9%	-5.8%	1.0%	0.5%
ρ_s = 0.09	Max	33.8%	28.8%	28.8%	35.1%	36.2%	39.7%	34.7%	48.3%	53.4%
	Avg.	15.5%	14.9%	14.9%	14.9%	18.6%	21.1%	12.4%	18.5%	25.7%
	Min	-2.4%	-4.9%	2.5%	-3.9%	-1.9%	0.6%	-4.0%	-3.3%	5.3%
ρ_s = 0.12	Max	29.1%	30.9%	30.9%	28.7%	30.6%	36.4%	29.2%	40.8%	47.7%
	Avg.	14.3%	14.9%	14.5%	13.5%	16.8%	19.2%	11.2%	15.8%	22.2%
	Min	-3.8%	-4.2%	0.0%	-1.9%	-1.0%	0.2%	-5.0%	-4.6%	-0.6%

loads. The maximum, minimum, and average errors for each bin are shown in Table 2-6 for the RCFT frames and anchor points computed using the PSD method, Table 2-7 for the SRC frames and anchor points computed using the PSD method, and Table 2-8 for SRC frames and anchor points computed using the MPSD method. The results in each table were obtained using the proposed interaction equation (Equation 1-17). A typical target maximum unconservative error for the development of stability design provisions is 5% (ASCE 1997) however current provisions result in greater errors for some cases (Denavit et al. 2016b). As shown in Table 2-6, the RCFT frames nearly achieve the target with a maximum unconservative (i.e., minimum ε) error over all cases of 5.6%. The maximum unconservative error for the SRC frames with anchor points computed using the PSD method is 17.9% (Table 2-7). This maximum error is for a case with a steel-dominant member (high steel ratio) and bending only about the *y*-axis, thus the error is primarily caused by unconservativness in the calculation of the anchor points not the proposed modification for biaxial bending. When computing the anchor points using the MPSD method, the maximum unconservative error for the SRC frames is 9.2% (Table 2-8). This maximum error is for a slender concrete-dominant member under high axial load, a region where high errors have been previously noted (Denavit et al. 2016b).

For both cross section types, the accuracy of the design methodology increases with steel ratio and slenderness. Some high conservative errors are noted, especially for concrete-dominant SRC frames. The largest of these errors are due to the shape of the design interaction strength equation, which neglects strength near the balance point. Development of methods of incorporating the balance point into the design interaction strength is recommended for future research. However, overall, the proposed design equation was found to have sufficient accuracy for design, particularly when paired with the MPSD method for SRC members.

Experimental Validation

The proposed interaction equation (Equation 1-17) results in greater available strength than the current equation. Despite being based on validated analytical models; it is prudent to validate the proposed equation against results of physical experiments as well. Thousands of experimental tests have been performed on steel-concrete composite columns (Goode 2008b; Gourley et al. 2008a), however, only a small fraction of these tests were conducted under biaxial loading.

Experimental data from tests on monotonically and biaxially loaded long composite columns was collected. In this work, long columns were defined as those having the slenderness ratio, λ as defined in Equation 1-19, greater than 8. A total of 11 RCFT specimens (Table 2-9) and 26 SRC specimens (Table 2-10) were identified in the literature. All specimens were subjected to eccentric loading and can be characterized as Type A frames (Figure 2-7) for analysis purposes in this work.

For each specimen, the maximum applied loads permitted by the design methodology (i.e., interaction surface 4) was computed following four separate methods as shown in Table 2-11. The methods varied in whether they were based on the current or proposed interaction strength equation and whether the anchor points were computed using the PSD method or MPSD method. A test-to-predicted ratio was computed for each specimen as the ratio of the radial distance from the origin to the experimental data point and the radial distance from the origin to interaction surface 4 (along the same line as to the experimental data point). An example interaction diagram is shown in Figure 2-10 which was computed based on Specimen 4 from Table 2-9. The computed test-to-predicted ratios are presented in Table 2-12 for the RCFT specimens and Table 2-13 for the SRC specimens. The results in Table 2-12 show that, for RCFT members, the proposed interaction equation increased the accuracy of the strength prediction compared to the current interaction equation by reducing the

Table 2-9. Properties of RCFT experimental specimens

Specimen No.	Specimen Label	H (mm)	B (mm)	t (mm)	L (mm)	λ	F_y (MPa)	f'_c (MPa)	Reference
1	SCH-3	200	200	9.91	2130	10.66	313	37.2	Bridge (1976)
2	SCH-4	200	200	9.91	2130	10.66	317	39.2	Bridge (1976)
3	SCH-5	200	200	9.91	3050	15.26	319	44.3	Bridge (1976)
4	SCH-6	200	200	9.91	3050	15.26	317	36.1	Bridge (1976)
5	M7	150	100	5.08	3210	26.19	347	39.3	Shakir-Khalil and Mouli (1990)
6	M9	150	100	5.08	3210	26.19	340	40.1	Shakir-Khalil and Mouli (1990)
7	R6	120	80	5.08	3210	32.78	343	38.3	Shakir-Khalil and Mouli (1990)
8	M2	120	80	5.08	3210	32.78	341	36.2	Shakir-Khalil and Mouli (1990)
9	M3	120	80	5.08	3210	32.78	341	39.3	Shakir-Khalil and Mouli (1990)
10	M4	120	80	5.08	3210	32.78	363	36.1	Shakir-Khalil and Mouli (1990)
11	M5	120	80	5.08	3210	32.78	363	34.7	Shakir-Khalil and Mouli (1990)

Table 2-10. Properties of SRC experimental specimens

Specimen No.	Specimen Label	H, B (mm)	ρ_s	ρ_{sr}	L (mm)	λ	F_y (MPa)	F_{ysr} (MPa)	f'_c (MPa)	Reference
1	CC5	150	0.04	0.004	1321	8.67	235	500	29.8	Tokgoz and Dunar (2008)
2	CC6	150	0.04	0.004	1321	8.67	235	500	34.0	Tokgoz and Dunar (2008)
3	D	254	0.05	0.004	3658	14.40	315	309	42.0	Virdi and Dowling (1973)
4	E	254	0.05	0.004	3658	14.40	315	309	39.6	Virdi and Dowling (1973)
5	F	254	0.05	0.004	3658	14.40	315	309	42.0	Virdi and Dowling (1973)
6	B4-30	160	0.09	0.002	2400	15.00	345	414	23.4	Morino et al. (1984b)
7	B4-45	160	0.09	0.002	2400	15.00	345	414	23.4	Morino et al. (1984b)
8	B4-60	160	0.09	0.002	2400	15.00	345	414	23.4	Morino et al. (1984b)
9	B8-30	160	0.09	0.002	2400	15.00	345	414	33.3	Morino et al. (1984b)
10	B8-45	160	0.09	0.002	2400	15.00	345	414	33.3	Morino et al. (1984b)
11	B8-60	160	0.09	0.002	2400	15.00	345	414	33.3	Morino et al. (1984b)
12	C4-30	160	0.09	0.002	3600	22.50	345	414	23.3	Morino et al. (1984b)
13	C4-45	160	0.09	0.002	3600	22.50	345	414	23.3	Morino et al. (1984b)
14	C4-60	160	0.09	0.002	3600	22.50	345	414	23.3	Morino et al. (1984b)
15	C8-30	160	0.09	0.002	3600	22.50	345	414	24.6	Morino et al. (1984b)
16	C8-45	160	0.09	0.002	3600	22.50	345	414	24.6	Morino et al. (1984b)
17	C8-60	160	0.09	0.002	3600	22.50	345	414	24.6	Morino et al. (1984b)
18	G	254	0.05	0.004	7315	28.80	315	309	36.4	Virdi and Dowling (1973)
19	H	254	0.05	0.004	7315	28.80	315	309	39.7	Virdi and Dowling (1973)
20	I	254	0.05	0.004	7315	28.80	315	309	43.2	Virdi and Dowling (1973)
21	D4-30	160	0.09	0.002	4801	30.00	345	414	21.2	Morino et al. (1984b)
22	D4-45	160	0.09	0.002	4801	30.00	345	414	21.2	Morino et al. (1984b)
23	D4-60	160	0.09	0.002	4801	30.00	345	414	21.2	Morino et al. (1984b)
24	D8-30	160	0.09	0.002	4801	30.00	345	414	22.9	Morino et al. (1984b)

Table 2-10 Continued

Specimen No.	Specimen Label	*H*, *B* (mm)	ρ_s	ρ_{sr}	*L* (mm)	λ	F_y (MPa)	F_{ysr} (MPa)	f'_c (MPa)	Reference
25	D8-45	160	0.09	0.002	4801	30.00	345	414	22.9	Morino et al. (1984b)
26	D8-60	160	0.09	0.002	4801	30.00	345	414	22.9	Morino et al. (1984b)

Table 2-11.The methods used for comparison to experimental data

Design Method	**Interaction Equation**	**Method for Computation of Anchor Points**
Method 1	Current (Equation 1-12)	PSD
Method 2	Proposed (Equation 1-17)	PSD
Method 3	Current (Equation 1-12)	MPSD
Method 4	Proposed (Equation 1-17)	MPSD

Table 2-12. Comparison of strength of RCFT experimental specimens

				Test-to-predicted ratio			
Specimen No.	P_{exp} (kN)	e_x (mm)	e_y (mm)	Method 1	Method 2	Method 3	Method 4
1	2180	19.00	32.91	1.14	1.05	1.15	1.06
2	2162	26.87	26.87	1.12	1.03	1.14	1.04
3	2037	19.00	32.91	1.03	0.96	1.05	0.97
4	1623	45.25	45.25	1.14	1.02	1.16	1.03
5	596.2	10.00	15.00	1.27	1.23	1.28	1.24
6	254.6	50.00	75.00	0.91	0.81	0.94	0.83
7	268	16.00	24.00	1.26	1.21	1.26	1.21
8	348	8.00	12.00	1.46	1.43	1.46	1.44
9	198.5	28.00	42.00	1.08	1.01	1.08	1.02
10	206.8	40.00	24.00	1.15	1.11	1.16	1.12
11	209.8	16.00	60.00	1.11	1.03	1.11	1.04
		Average		1.15	1.08	1.16	1.09
		Standard Deviation		0.14	0.16	0.14	0.16

Table 2-13. Comparison of strength of SRC experimental specimens

				Test-to-predicted ratio			
Specimen No.	P_{exp} (kN)	e_x (mm)	e_y (mm)	Method 1	Method 2	Method 3	Method 4
1	185.00	50.00	50.00	1.39	1.21	1.45	1.26
2	208.00	55.00	55.00	1.66	1.45	1.71	1.49
3	927.07	63.50	36.83	1.05	0.95	1.13	1.01
4	573.19	127.00	73.66	1.31	1.15	1.43	1.26
5	418.67	190.50	110.49	1.41	1.24	1.53	1.35
6	392.47	34.64	20.00	0.92	0.88	1.03	0.97
7	389.49	28.29	28.29	0.90	0.85	1.00	0.94
8	436.24	20.00	34.64	0.97	0.91	1.07	1.00
9	263.51	64.95	37.50	0.84	0.74	1.02	0.90
10	294.21	53.03	53.03	0.93	0.81	1.14	0.99
11	328.32	37.50	64.95	0.97	0.85	1.18	1.03
12	283.44	34.64	20.00	0.96	0.94	1.03	1.00
13	304.35	28.29	28.29	1.02	0.98	1.09	1.05
14	340.16	20.00	34.64	1.09	1.05	1.17	1.12
15	176.42	64.95	37.50	0.73	0.70	0.83	0.78
16	195.28	53.03	53.03	0.80	0.75	0.90	0.83
17	194.03	37.50	64.95	0.75	0.71	0.84	0.78
18	667.52	63.50	36.83	1.44	1.39	1.49	1.44
19	353.69	127.00	73.66	1.00	0.94	1.05	0.98
20	293.91	190.50	110.49	1.05	0.96	1.12	1.02
21	200.88	34.64	20.00	1.07	1.05	1.12	1.10
22	209.02	28.29	28.29	1.09	1.07	1.15	1.12
23	219.88	20.00	34.64	1.11	1.08	1.17	1.13
24	117.30	64.95	37.50	0.71	0.69	0.77	0.74
25	146.61	53.03	53.03	0.88	0.85	0.94	0.90
26	158.36	37.50	64.95	0.91	0.87	0.98	0.93
	Average			1.04	0.96	1.13	1.04
	Standard Deviation			0.23	0.20	0.23	0.19

conservative error by 7% on average. Use of the MPSD method has little effect for RCFT members, increasing conservative error by 1% on average.

The average test-to-predicted ratios are closer to unity for the SRC members. As shown in Table 2-13, when using the PSD method to compute the anchor points, the current interaction equation shows a conservative error of 4% on average while the proposed interaction equation shows an unconservative error of 4% on average. It is notable that the precision of the proposed interaction equation is higher with a standard deviation on the test-to-predicted ratio of 0.20 compared to 0.23 for the current interaction equation. Use of the MPSD method to compute the anchor points shift the results to the conservative side. The proposed interaction equation with the MPSD method shows the best results of those investigated with an average test-to-predicted ratio of 1.04 and standard deviation of 0.19.

Conclusions

Previous studies have shown that steel-concrete composite columns maintain most of their uniaxial strength when subjected to biaxial bending. This behavior suggests that these members have a more convex strength interaction diagram than the diamond-shaped strength interaction diagram currently recommended in the commentary on the AISC *Specification* (2016). A broad parametric study was performed to assess the strength of steel-concrete composite cross sections subjected to axial compression and biaxial bending with the goal of developing new recommendations with increased strength and improved accuracy while maintaining simplicity. Three-dimensional strength interaction diagrams were computed for a parametric suite of thousands of composite cross sections using the plastic stress distribution (PSD) and strain compatibility (SC) design methods as well as with fiber-based inelastic section analyses (ISA).

The shape of the interaction diagrams, computed using each of the three methods, was quantified by fitting them to a generalized elliptical interaction equation. The shape was noted to vary with cross-sectional parameters, axial load, and method. The generalized interaction equation was proposed for design with a recommended shape parameter for each section type based on the minimum best fit α computed using the ISA method.

The proposed interaction equation was verified against second-order inelastic analyses of a suite of columns with various steel ratios, concrete strengths, slenderness ratios, end restraints, and frame types. It was also validated against published experimental results. These comparisons demonstrated that the proposed interaction equation is suitable for use within the direct analysis method as defined in the AISC *Specification* (2016), especially when used in conjunction with anchor points computed using a modified version of the plastic stress distribution method.

References

Abdel-Rahman, N., and Sivakumaran, K. S. (1997). “Material properties models for analysis of cold-formed steel members.” *Journal of Structural Engineering*, 123, 1135–1143.

ACI. (2014). *Building Code Requirements for Structural Concrete and Commentary*. American Concrete Institute, Farmington Hills, MI.

ACI. (2018). *Report on Equivalent Rectangular Concrete Stress Block and Transverse Reinforcement for High-Strength Concrete Columns*. 441.1R-18, ACI.

ACI. (2019). *Building Code Requirements for Structural Concrete and Commentary*. American Concrete Institute, Farmington Hills, MI.

AISC. (1986). *Load and Resistance Factor Design Specification for Structural Steel Buildings*. American Institute of Steel Construction, Chicago, Illinois.

AISC. (2005). *Specification for Structural Steel Buildings*. American Institute of Steel Construction, Chicago, Illinois.

AISC. (2016). *Specification for structural steel buildings*. American Institute of Steel Construction, Chicago, Illinois.

AISC. (2017). *Steel Construction Manual, 15th Edition*. American Institute of Steel Construction, Chicago, Illinois.

ASCE. (1997). *Effective Length and Notional Load Approaches for Assessing Frame Stability: Implications for American Steel Design*. American Society of Civil Engineers, Reston, Virginia.

ASTM A6. (2019). *ASTM A6/A6M-11: Standard Specification for General Requirements for Rolled Structural Steel Bars, Plates, Shapes and Sheet Piling*. ASTM International West Conshohocken, PA.

ASTM A500. (2020). *ASTM A500/A500M: Standard Specification for Cold-Formed Welded and Seamless Carbon Steel Structural Tubing in Rounds and Shapes*. ASTM International West Conshohocken, PA.

ASTM A615. (2020). *ASTM A615/A615M: Standard Specification for Deformed and Plain Carbon-Steel Bars for Concrete Reinforcement*. ASTM International West Conshohocken, PA.

Behnam, A., and Denavit, M. D. (2020). “Plastic stress distribution method for predicting interaction strength of steel-concrete composite cross sections.” *Journal of Constructional Steel Research*, 170, 106092.

Brent, R. P. (2013). *Algorithms for minimization without derivatives*. Courier Corporation.

Bridge, R. Q. (1976). *Concrete filled steel tubular columns*. School of Civil Engineering, University of Sydney, Sydney, Australia.

CEN. (2004). *Eurocode 4: Design of composite steel and concrete structures—Part 1.1: General rules and rules for buildings*. European Committee for Standardization, Brussels, Belgium.

Chen, C.-C. (2012). “Accuracy of AISC methods in predicting flexural strength of concrete-encased members.” *Journal of Structural Engineering*, 139(3), 338–349.

Denavit, M. D., and Hajjar, J. F. (2014). *Characterization of Behavior of Steel-Concrete Composite Members and Frames with Applications for Design*. Newmark Structural Laboratory Report Series, Newmark Structural Laboratory Report NSEL-034, University of Illinois at Urbana-Champaign, Urbana, Illinois.

Denavit, M. D., Hajjar, J. F., Perea, T., and Leon, R. T. (2016a). “Stability Analysis and Design of Composite Structures.” *Journal of Structural Engineering*, ASCE, 142(3), 04015157.

Denavit, M. D., Hajjar, J. F., Perea, T., and Leon, R. T. (2016b). “Stability analysis and design of composite structures.” *Journal of Structural Engineering*, 142, 1–12.

Dixon, L. C. W. (1978). “The global optimization problem. an introduction.” *Toward global optimization*, 2, 1–15.

Forsythe, G. E., Malcolm, M. A., and Moler, C. B. (1977). *Computer Methods for Mathematical Computations*. Prentice Hall.

Fujikura, S., Bruneau, M., and Lopez-Garcia, D. (2008). “Experimental investigation of multihazard resistant bridge piers having concrete-filled steel tube under blast loading.” *Journal of Bridge Engineering*, 13, 586–594.

Furlong, R. W., Hsu, C.-T. T., and Mirza, S. A. (2004). “Analysis and design of concrete columns for biaxial bending-overview.” *Structural Journal*, 101(3), 413–422.

Galambos, T. V., and Ketter, R. L. (1959). “Columns under combined bending and thrust.” *Journal of the Engineering Mechanics Division*, 85(2), 1–30.

Goode, C. D. (2008a). “Composite Columns - 1819 Tests on Concrete-Filled Steel Tube Columns Compared with Eurocode 4.” *The Structural Engineer*, 86(16), 33–38.

Goode, C. D. (2008b). “Composite columns-1819 tests on concrete-filled steel tube columns compared with Eurocode 4.” *The Structural Engineer*, 86, 33–38.

Gourley, B. C., Tort, C., Denavit, M. D., Schiller, P. H., and Hajjar, J. F. (2008a). *A synopsis of studies of the monotonic and cyclic behavior of concrete-filled steel tube members, connections, and frames*. Newmark Structural Engineering Laboratory. University of Illinois at Urbana-Champaign.

Gourley, B. C., Tort, C., Denavit, M. D., Schiller, P. H., and Hajjar, J. F. (2008b). *A Synopsis of Studies of the Monotonic and Cyclic Behavior of Concrete-Filled Steel Tube Members, Connections, and Frames*. Newmark Structural Laboratory Report NSEL-008, Department of Civil and Environmental Engineering, University of Illinois at Urbana-Champaign, Urbana, Illinois.

Griffis, L. G. (1992). *Load and Resistance Factor Design of W-Shapes Encased in Concrete*. Design Guide 6, American Institute of Steel Construction, Chicago, Illinois.

Hardika, M. S., and Gardner, N. J. (2004). “Behavior of concrete-filled hollow structural section beam columns to seismic shear displacements.” *Structural Journal*, 101, 39–46.

Hatzigeorgiou, G. D. (2008). “Numerical model for the behavior and capacity of circular CFT columns, Part I: Theory.” *Engineering Structures*, 30(6), 1573–1578.

Kanchanalai, T. (1977). *The Design and Behavior of Beam-Columns in Unbraced Steel Frames*. CESRL Report No. 77-2, Structures Research Laboratory, Department of Civil Engineering, The University of Texas at Austin, Austin, Texas.

Kim, D. K. (2005). “A Database for Composite Columns.” M.S. Thesis, School of Civil and Environmental Engineering, Georgia Institute of Technology, Atlanta, Georgia.

Kostic, S. M., and Filippou, F. C. (2012). “Section discretization of fiber beam-column elements for cyclic inelastic response.” *Journal of Structural Engineering*, American Society of Civil Engineers, 138(5), 592–601.

Lai, Z., and Varma, A. H. (2015). “Noncompact and slender circular CFT members: Experimental database, analysis, and design.” *Journal of Constructional Steel Research*, 106, 220–233.

Lai, Z., and Varma, A. H. (2016). “Effective stress-strain relationships for analysis of noncompact and slender filled composite (CFT) members.” *Engineering Structures*, Elsevier, 124, 457–472.

Lai, Z., Varma, A. H., and Zhang, K. (2014). “Noncompact and slender rectangular CFT members: Experimental database, analysis, and design.” *Journal of Constructional Steel Research*, 101, 455–468.

Leon, R. T., Kim, D. K., and Hajjar, J. F. (2007). “Limit State Response of Composite Columns and Beam-Columns Part 1: Formulation of Design Provisions for the 2005 AISC Specification.” *Engineering Journal*, AISC, 44(4), 341–358.

Liang, Q. Q. (2008). “Nonlinear analysis of short concrete-filled steel tubular beam–columns under axial load and biaxial bending.” *Journal of Constructional Steel Research*, 64(3), 295–304.

Liang, Q. Q., Patel, V. I., and Hadi, M. N. (2012). “Biaxially loaded high-strength concrete-filled steel tubular slender beam-columns, Part I: Multiscale simulation.” *Journal of Constructional Steel Research*, 75, 64–71.

MacGregor, J. G., and Hage, S. E. (1977). “Stability Analysis and Design of Concrete Frames.” *Journal of the Structural Division, ASCE*, 103(10), 1953–1970.

McKenna, F., Scott, M. H., and Fenves, G. L. (2010a). “Nonlinear finite-element analysis software architecture using object composition.” *Journal of Computing in Civil Engineering*, 24(1), 95–107.

McKenna, F., Scott, M. H., and Fenves, G. L. (2010b). “Nonlinear Finite-Element Analysis Software Architecture Using Object Composition.” *Journal of Computing in Civil Engineering*, ASCE, 24(1), 95–107.

Morino, S., Matsui, C., and Watanabe, H. (1984a). "Strength of biaxially loaded SRC columns." 185–194.

Morino, S., Matsui, C., and Watanabe, H. (1984b). "Strength of Biaxially Loaded SRC Columns." *Composite and Mixed Construction*, American Society of Civil Engineers, 185–194.

Patel, V. I., Liang, Q. Q., and Hadi, M. N. (2015). "Biaxially loaded high-strength concrete-filled steel tubular slender beam-columns, Part II: Parametric study." *Journal of Constructional Steel Research*, 110, 200–207.

Perea, T., Leon, R. T., Hajjar, J. F., and Denavit, M. D. (2014). "Full-scale tests of slender concrete-filled tubes: Interaction behavior." *Journal of Structural Engineering*, 140, 04014054.

Ricles, J. M., and Paboojian, S. D. (1994). "Seismic performance of steel-encased composite columns." *Journal of Structural Engineering*, 120, 2474–2494.

SAC. (2014). *Technical code for concrete filled steel tubular structures, GB 50936-2014*. Standardization Administration of the People's Republic of China, Beijing.

Sakino, K., Nakahara, H., Morino, S., and Nishiyama, I. (2004). "Behavior of centrally loaded concrete-filled steel-tube short columns." *Journal of Structural Engineering*, 130, 180–188.

Sanz Picon, C. F. (1992). "Behavior of composite column cross sections under biaxial bending." MS.c. Thesis, Cornell University, Ithaca, New York.

Shakir-Khalil, H., and Mouli, M. (1990). "Further Tests on Concrete-Filled Rectangular Hollow-section columns." *The Structural Engineer*, 68, 9.

Shakir-Khalil, H., and Zeghiche, J. (1989). "Experimental Behaviour of Concrete-Filled Rolled Rectangular Hollow-Section Columns." *The Structural Engineer*, 67, 346–354.

Surovek-Maleck, A. E., and White, D. W. (2004). "Alternative approaches for elastic analysis and design of steel frames. I: Overview." *Journal of Structural Engineering*, 130, 1186–1196.

Tokgoz, S., and Dundar, C. (2008). "Experimental tests on biaxially loaded concrete-encased composite columns." *Steel and Composite Structures*, 8(5), 423–438.

Tomii, M., and Sakino, K. (1979). "Experimental studies on the ultimate moment of concrete filled square steel tubular beam-columns." *Transactions of the Architectural Institute of Japan*, 275, 55–65.

Ugray, Z., Lasdon, L., Plummer, J., Glover, F., Kelly, J., and Martí, R. (2007). "Scatter search and local NLP solvers: A multistart framework for global optimization." *INFORMS Journal on Computing*, 19(3), 328–340.

Varma, A. H., Ricles, J. M., Sause, R., and Lu, L.-W. (2002). "Seismic behavior and modeling of high-strength composite concrete-filled steel tube (CFT) beam–columns." *Journal of Constructional Steel Research*, 58, 725–758.

Virdi, K. S., and Dowling, P. J. (1973). "The Ultimate Strength of Composite Columns in Biaxial Bending." *Proceedings of the Institution of Civil Engineers*, 55(1), 251–272.

Virdi, K. S., Pilkington, J., Dowling, P., and Croft, D. (1973). “Discussion. The ultimate strength of composite columns in biaxial bending.” *Proceedings of the institution of civil engineers*, 55, 739–741.

CONCLUSION

The plastic stress distribution (PSD) method is commonly used for calculating the strength of steel-concrete composite column cross sections. While the accuracy of this method has been evaluated for some cases, no previous study has systematically evaluated its accuracy over the whole range of materials, cross-sectional geometries, and loading conditions for which it is permitted to be applied. In the first part of this thesis, a broad parametric study was performed to assess the strength of steel-concrete composite cross sections subjected to axial compression and uniaxial/biaxial bending to evaluate the PSD method. For this purpose, three-dimensional strength interaction diagrams were computed for a parametric suite of thousands of composite cross sections using the PSD and strain compatibility (SC) methods as well as with a fiber-based inelastic section analysis (ISA). In comparison to the ISA method, the SC method was found to be conservative, predicting lower strengths in almost all cases. The PSD method, on the other hand, was found to produce unconservative errors for some cross sections. For SRC cross sections, this error was greatest with high steel ratios and high steel yield stresses, with unconservative error as much as 38% in *y*-axis bending and 29% in *x*-axis bending. For RCFT cross sections, the maximum unconservative error was found to be about 14% which occurred for cross sections with high steel yield stress. For CCFT cross sections, the maximum unconservative error was found to be about 1%. A simple modification to the PSD method was proposed to reduce the unconservative error in SRC and RCFT cross sections. This modification was calibrated based on inelastic section analysis results. With the modification, the 95th percentile of unconservative error in the broad range of cross sections examined was reduced to less than 5%, while the maximum conservative error increased slightly. Validation against published experimental results confirmed that the PSD method overestimates the strength for some cross sections and that the modified PSD method provides improved accuracy.

In the second part of this thesis, the behavior and design of composite members under biaxial flexure and axial compression including length effects are investigated. Previous studies have shown that steel-concrete composite columns maintain most of their uniaxial strength when subjected to biaxial bending. This behavior suggests that these members have a more convex strength interaction diagram than the diamond-shaped strength interaction diagram currently recommended in the commentary on the AISC *Specification* (2016). A broad parametric study was performed to assess the strength of steel-concrete composite cross sections subjected to axial compression and biaxial bending with the goal of developing new recommendations with increased strength and improved accuracy while maintaining simplicity. Three-dimensional strength interaction diagrams were computed for a parametric suite of thousands of composite cross sections using the PSD, SC, and ISA methods. The shape of the interaction diagrams, computed using each of the three methods, was quantified by fitting them to a generalized elliptical interaction equation. The shape was noted to vary with cross-sectional parameters, axial load, and method. The generalized interaction equation was proposed for design with a recommended shape parameter, α, for each section type based on the minimum best fit α computed using the ISA method. The proposed interaction equation was verified against second-order inelastic analyses of a suite of columns with various steel ratios, concrete strengths, slenderness ratios, end restraints, and frame types. It was also validated against published experimental results. These comparisons demonstrated that the proposed interaction equation is suitable for use within the direct analysis method as defined in the AISC *Specification* (2016), especially when used in conjunction with anchor points computed using the modified version of the PSD method developed in the first part of this thesis.

In this work, the behavior and strength of steel-concrete composite members was studied under uniaxial and biaxial bending and axial compression, and the design methodologies presented in the AISC *Specification* (2016) for the calculation of the strength of these members was evaluated and modified to improve the accuracy where the PSD method yields unconservative results, and where the equation for biaxial bending strength is overly conservative. The results of this work will enable more efficient designs of steel-concrete composite columns.

References

AISC. (2016). *Specification for structural steel buildings*. American Institute of Steel Construction, Chicago, Illinois.

VITA

Amirfarzad Behnam was born in Tehran, Iran. He started his Bachelor of Science in Civil Engineering at the Iran University of Science and Technology, Tehran, Iran. After completing his BSc, in the same year he got admitted to the department of Earthquake Engineering at Building and Construction Research Institute, Tehran, Iran for his Master of Science program in Earthquake Engineering and finished his study in 2011. After completing his master thesis titled “Design optimization of reinforced concrete 3D structures considering frequency constraints via a charged system search”, Amirfarzad started working as structural engineer for 2 years in industry before getting admitted for a PhD program in the department of Civil Engineering at the Ferdowsi University of Mashhad, Iran.

In 2017, Amirfarzad served as a visiting scholar for six months at the university of Tennessee, Knoxville and after obtaining his PhD from Ferdowsi University of Mashhad, he moved to the United States to pursue his research interests as a PhD student in the Structural Engineering department at the University of Tennessee, Knoxville in the Spring of 2018.